THE TENTH DATA RELEASE OF THE SLOAN DIGITAL SKY SURVEY: FIRST SPECTROSCOPIC DATA FROM THE SDSS-III APACHE POINT OBSERVATORY GALACTIC EVOLUTION EXPERIMENT

Christopher P. Ahn[1], Rachael Alexandroff[2], Carlos Allende Prieto[3,4], Friedrich Anders[5,6], Scott F. Anderson[7], Timothy Anderton[1], Brett H. Andrews[8], Éric Aubourg[9], Stephen Bailey[10], Fabienne A. Bastien[11], Julian E. Bautista[9], Timothy C. Beers[12,13], Alessandra Beifiori[14], Chad F. Bender[15,16] Andreas A. Berlind[11], Florian Beutler[10], Vaishali Bhardwaj[7,10], Jonathan C. Bird[11], Dmitry Bizyaev[17,18], Cullen H. Blake[19], Michael R. Blanton[20], Michael Blomqvist[21], John J. Bochanski[22,7], Adam S. Bolton[1], Arnaud Borde[23], Jo Bovy[24,25], Alaina Shelden Bradley[17], W. N. Brandt[15,26], Dorothée Brauer[5], J. Brinkmann[17], Joel R. Brownstein[1], Nicolás G. Busca[9], William Carithers[10], Joleen K. Carlberg[27], Aurelio R. Carnero[28,29], Michael A. Carr[30], Cristina Chiappini[5,29], S. Drew Chojnowski[31], Chia-Hsun Chuang[32], Johan Comparat[33], Justin R. Crepp[34], Stefano Cristiani[35,36], Rupert A.C. Croft[37], Antonio J. Cuesta[38], Katia Cunha[28,39], Luiz N. da Costa[28,29], Kyle S. Dawson[1], Nathan De Lee[11], Janice D. R. Dean[31], Timothée Delubac[23], Rohit Deshpande[15,16], Saurav Dhital[40,11], Anne Ealet[41], Garrett L. Ebelke[17,18], Edward M. Edmondson[42], Daniel J. Eisenstein[43], Courtney R. Epstein[8], Stephanie Escoffier[41], Massimiliano Esposito[3,4], Michael L. Evans[7], D. Fabbian[3], Xiaohui Fan[39], Ginevra Favole[32], Bruno Femenía Castellá[3,4], Emma Fernández Alvar[3,4], Diane Feuillet[18], Nurten Filiz Ak[15,26,44], Hayley Finley[45], Scott W. Fleming[15,16], Andreu Font-Ribera[46,10], Peter M. Frinchaboy[47], J. G. Galbraith-Frew[1], D. A. García-Hernández[3,4], Ana E. García Pérez[31], Jian Ge[48], R. Génova-Santos[3,4], Bruce A. Gillespie[2,17], Léo Girardi[49,29], Jonay I. González Hernández[3], J. Richard Gott, III[30], James E. Gunn[30], Hong Guo[1], Samuel Halverson[15], Paul Harding[50], David W. Harris[1], Sten Hasselquist[18], Suzanne L. Hawley[7], Michael Hayden[18], Frederick R. Hearty[31], Artemio Herrero Davó[3,4], Shirley Ho[37], David W. Hogg[20], Jon A. Holtzman[18], Klaus Honscheid[51,52], Joseph Huehnerhoff[17], Inese I. Ivans[1], Kelly M. Jackson[47,53], Peng Jiang[54,48], Jennifer A. Johnson[8,52], K. Kinemuchi[17,18], David Kirkby[21], Mark A. Klaene[17], Jean-Paul Kneib[55,33], Lars Koesterke[56], Ting-Wen Lan[2], Dustin Lang[37], Jean-Marc Le Goff[23], Alexie Leauthaud[57], Khee-Gan Lee[58], Young Sun Lee[18], Daniel C. Long[17,18], Craig P. Loomis[30], Sara Lucatello[49], Robert H. Lupton[30], Bo Ma[48], Claude E. Mack III[11], Suvrath Mahadevan[15,16], Marcio A. G. Maia[28,29], Steven R. Majewski[31], Elena Malanushenko[17,18], Viktor Malanushenko[17,18], A. Manchado[3,4], Marc Manera[42], Claudia Maraston[42], Daniel Margala[21], Sarah L. Martell[59], Karen L. Masters[42], Cameron K. McBride[43], Ian D. McGreer[39], Richard G. McMahon[60,61], Brice Ménard[2,57,62], Sz. Mészáros[3,4], Jordi Miralda-Escudé[63,64], Hironao Miyatake[30], Antonio D. Montero-Dorta[1], Francesco Montesano[14], Surhud More[57], Heather L. Morrison[50], Demitri Muna[8], Jeffrey A. Munn[65], Adam D. Myers[66], Duy Cuong Nguyen[67], Robert C. Nichol[42], David L. Nidever[68,31], Pasquier Noterdaeme[45], Sebastián E. Nuza[5], Julia E. O'Connell[47], Robert W. O'Connell[31], Ross O'Connell[37], Matthew D. Olmstead[1], Daniel J. Oravetz[17], Russell Owen[7], Nikhil Padmanabhan[38], Nathalie Palanque-Delabrouille[23], Kaike Pan[17], John K. Parejko[38], Prachi Parihar[11], Isabelle Pâris[69], Joshua Pepper[70,11], Will J. Percival[42], Ignasi Pérez-Ràfols[64,71], Hélio Dotto Perottoni[72,29], Patrick Petitjean[45], Matthew M. Pieri[42], M. H. Pinsonneault[8], Francisco Prada[73,32,74], Adrian M. Price-Whelan[75], M. Jordan Raddick[2], Mubdi Rahman[2], Rafael Rebolo[3,76], Beth A. Reid[10,25], Jonathan C. Richards[1], Rogério Riffel[77,29], Annie C. Robin[78], H. J. Rocha-Pinto[72,29], Constance M. Rockosi[79], Natalie A. Roe[10], Ashley J. Ross[42], Nicholas P. Ross[10], Graziano Rossi[23], Arpita Roy[15], J. A. Rubiño-Martin[3,4], Cristiano G. Sabiu[80], Ariel G. Sánchez[14], Basílio Santiago[77,29], Conor Sayres[7], Ricardo P. Schiavon[81], David J. Schlegel[10], Katharine J. Schlesinger[82], Sarah J. Schmidt[8], Donald P. Schneider[15,26], Mathias Schultheis[78], Kris Sellgren[8], Hee-Jong Seo[10], Yue Shen[43,83], Matthew Shetrone[84], Yiping Shu[1], Audrey E. Simmons[17], M. F. Skrutskie[31], Anže Slosar[85], Verne V. Smith[12], Stephanie A. Snedden[17], Jennifer S. Sobeck[86], Flavia Sobreira[28,29], Keivan G. Stassun[11,87], Matthias Steinmetz[5], Michael A. Strauss[30,88], Alina Streblyanska[3,4], Nao Suzuki[10], Molly E. C. Swanson[43], Ryan C. Terrien[15,16], Aniruddha R. Thakar[2], Daniel Thomas[42], Benjamin A. Thompson[47], Jeremy L. Tinker[20], Rita Tojeiro[42], Nicholas W. Troup[31], Jan Vandenberg[2], Mariana Vargas Magaña[37], Matteo Viel[35,36], Nicole P. Vogt[18], David A. Wake[89], Benjamin A. Weaver[20], David H. Weinberg[8], Benjamin J. Weiner[39], Martin White[90,10], Simon D.M. White[91], John C. Wilson[31], John P. Wisniewski[92], W. M. Wood-Vasey[93,88], Christophe Yèche[23], Donald G. York[94], O. Zamora[3,4], Gail Zasowski[8,2], Idit Zehavi[50], Gong-Bo Zhao[42,95], Zheng Zheng[1], Guangtun Zhu[2]

Draft version January 16, 2014

ABSTRACT

The Sloan Digital Sky Survey (SDSS) has been in operation since 2000 April. This paper presents the tenth public data release (DR10) from its current incarnation, SDSS-III. This data release includes the first spectroscopic data from the Apache Point Observatory Galaxy Evolution Experiment (APOGEE), along with spectroscopic data from the Baryon Oscillation Spectroscopic Survey (BOSS) taken through 2012 July. The APOGEE instrument is a near-infrared $R \sim 22,500$ 300-fiber spectrograph covering 1.514–1.696 μm. The APOGEE survey is studying the chemical abundances and radial velocities of roughly 100,000 red giant star candidates in the bulge, bar, disk, and halo of the Milky Way. DR10 includes 178,397 spectra of 57,454 stars, each typically observed three or more times, from APOGEE. Derived quantities from these spectra (radial velocities, effective temperatures, surface gravities, and metallicities) are also included.

DR10 also roughly doubles the number of BOSS spectra over those included in the ninth data release. DR10 includes a total of 1,507,954 BOSS spectra, comprising 927,844 galaxy spectra; 182,009 quasar spectra; and 159,327 stellar spectra, selected over 6373.2 deg^2.

1. INTRODUCTION

The Sloan Digital Sky Survey (SDSS) has been in continuous operation since 2000 April. It uses a dedicated

[1] Department of Physics and Astronomy, University of Utah, Salt Lake City, UT 84112, USA.

[2] Center for Astrophysical Sciences, Department of Physics and Astronomy, Johns Hopkins University, 3400 North Charles Street, Baltimore, MD 21218, USA.

[3] Instituto de Astrofísica de Canarias (IAC), C/Vía Láctea, s/n, E-38200, La Laguna, Tenerife, Spain.

[4] Departamento de Astrofísica, Universidad de La Laguna, E-38206, La Laguna, Tenerife, Spain.

[5] Leibniz-Institut für Astrophysik Potsdam (AIP), An der Sternwarte 16, D-14482 Potsdam, Germany.

[6] Technische Universität Dresden (TUD), Institut für Kern- und Teilchenphysik, D-01062 Dresden, Germany.

[7] Department of Astronomy, University of Washington, Box 351580, Seattle, WA 98195, USA.

[8] Department of Astronomy, Ohio State University, 140 West 18th Avenue, Columbus, OH 43210, USA.

[9] APC, University of Paris Diderot, CNRS/IN2P3, CEA/IRFU, Observatoire de Paris, Sorbonne Paris Cité, F-75205 Paris, France.

[10] Lawrence Berkeley National Laboratory, One Cyclotron Road, Berkeley, CA 94720, USA.

[11] Department of Physics and Astronomy, Vanderbilt University, VU Station 1807, Nashville, TN 37235, USA.

[12] National Optical Astronomy Observatory, 950 North Cherry Avenue, Tucson, AZ, 85719, USA.

[13] Department of Physics and Astronomy and JINA: Joint Institute for Nuclear Astrophysics, Michigan State University, East Lansing, MI 48824, USA.

[14] Max-Planck-Institut für Extraterrestrische Physik, Giessenbachstraße, D-85748 Garching, Germany.

[15] Department of Astronomy and Astrophysics, 525 Davey Laboratory, The Pennsylvania State University, University Park, PA 16802, USA.

[16] Center for Exoplanets and Habitable Worlds, 525 Davey Laboratory, Pennsylvania State University, University Park, PA 16802, USA.

[17] Apache Point Observatory, P.O. Box 59, Sunspot, NM 88349, USA.

[18] Department of Astronomy, MSC 4500, New Mexico State University, P.O. Box 30001, Las Cruces, NM 88003, USA.

[19] University of Pennsylvania, Department of Physics and Astronomy, 219 S. 33rd St., Philadelphia, PA 19104.

[20] Center for Cosmology and Particle Physics, Department of Physics, New York University, 4 Washington Place, New York, NY 10003, USA.

[21] Department of Physics and Astronomy, University of California, Irvine, CA 92697, USA.

[22] Haverford College, Department of Physics and Astronomy, 370 Lancaster Avenue, Haverford, PA, 19041, USA.

[23] CEA, Centre de Saclay, Irfu/SPP, F-91191 Gif-sur-Yvette, France.

[24] Institute for Advanced Study, Einstein Drive, Princeton, NJ 08540, USA.

[25] Hubble fellow.

[26] Institute for Gravitation and the Cosmos, The Pennsylvania State University, University Park, PA 16802, USA.

[27] Department of Terrestrial Magnetism, Carnegie Institution of Washington, 5241 Broad Branch Road, NW, Washington DC 20015, USA.

[28] Observatório Nacional, Rua Gal. José Cristino 77, Rio de Janeiro, RJ - 20921-400, Brazil.

[29] Laboratório Interinstitucional de e-Astronomia, - LIneA, Rua Gal.José Cristino 77, Rio de Janeiro, RJ - 20921-400, Brazil.

[30] Department of Astrophysical Sciences, Princeton University, Princeton, NJ 08544, USA.

[31] Department of Astronomy, University of Virginia, P.O.Box 400325, Charlottesville, VA 22904-4325, USA.

[32] Instituto de Física Teórica, (UAM/CSIC), Universidad Autónoma de Madrid, Cantoblanco, E-28049 Madrid, Spain.

[33] Laboratoire d'Astrophysique de Marseille, CNRS-Université de Provence, 38 rue F. Joliot-Curie, F-13388 Marseille cedex 13, France.

[34] Department of Physics, 225 Nieuwland Science Hall, Notre Dame, IN, 46556, USA.

[35] INAF, Osservatorio Astronomico di Trieste, Via G. B. Tiepolo 11, I-34131 Trieste, Italy.

[36] INFN/National Institute for Nuclear Physics, Via Valerio 2, I-34127 Trieste, Italy.

[37] Bruce and Astrid McWilliams Center for Cosmology, Department of Physics, Carnegie Mellon University, 5000 Forbes Ave, Pittsburgh, PA 15213, USA.

[38] Yale Center for Astronomy and Astrophysics, Yale University, New Haven, CT, 06520, USA.

[39] Steward Observatory, 933 North Cherry Avenue, Tucson, AZ 85721, USA.

[40] Department of Physical Sciences, Embry-Riddle Aeronautical University, 600 South Clyde Morris Blvd., Daytona Beach, FL 32114, USA.

[41] Centre de Physique des Particules de Marseille, Aix-Marseille Université, CNRS/IN2P3, E-13288 Marseille, France.

[42] Institute of Cosmology and Gravitation, Dennis Sciama Building, University of Portsmouth, Portsmouth, PO1 3FX, UK.

[43] Harvard-Smithsonian Center for Astrophysics, Harvard University, 60 Garden Street, Cambridge MA 02138, USA.

[44] Faculty of Sciences, Department of Astronomy and Space Sciences, Erciyes University, 38039 Kayseri, Turkey.

[45] UPMC-CNRS, UMR7095, Institut d'Astrophysique de Paris, 98bis Boulevard Arago, F-75014, Paris, France.

[46] Institute of Theoretical Physics, University of Zurich, 8057 Zurich, Switzerland.

[47] Department of Physics and Astronomy, Texas Christian University, 2800 South University Drive, Fort Worth, TX 76129, USA.

[48] Department of Astronomy, University of Florida, Bryant Space Science Center, Gainesville, FL 32611-2055, USA.

[49] INAF, Osservatorio Astronomico di Padova, Vicolo dell'Osservatorio 5, I-35122 Padova, Italy.

[50] Department of Astronomy, Case Western Reserve University, Cleveland, OH 44106, USA.

[51] Department of Physics, Ohio State University, Columbus, OH 43210, USA.

[52] Center for Cosmology and Astro-Particle Physics, Ohio State University, Columbus, OH 43210, USA.

[53] Department of Physics, University of Texas-Dallas, Dallas, TX 75080, USA.

[54] Key Laboratory for Research in Galaxies and Cosmology, University of Science and Technology of China, Chinese Academy of Sciences, Hefei, Anhui, 230026, China.

[55] Laboratoire d'Astrophysique, École Polytechnique Fédérale de Lausanne (EPFL), Observatoire de Sauverny, 1290, Versoix, Switzerland.

[56] Texas Advanced Computer Center, University of Texas, 10100 Burnet Road (R8700), Austin, Texas 78758-4497, USA.

[57] Kavli Institute for the Physics and Mathematics of the Universe (Kavli IPMU, WPI), Todai Institutes for Advanced Study, The University of Tokyo, Kashiwa, 277-8583, Japan.

[58] Max-Planck-Institut für Astronomie, Königstuhl 17, D-69117 Heidelberg, Germany.

[59] Australian Astronomical Observatory, PO Box 915, North Ryde NSW 1670, Australia.

[60] Institute of Astronomy, University of Cambridge, Madingley Road, Cambridge CB3 0HA, UK.

[61] Kavli Institute for Cosmology, University of Cambridge, Madingley Road, Cambridge CB3 0HA, UK.

wide-field 2.5-m telescope (Gunn et al. 2006) at Apache Point Observatory (APO) in the Sacramento Mountains in Southern New Mexico. It was originally instrumented with a wide-field imaging camera with an effective area of 1.5 deg^2 (Gunn et al. 1998), and a pair of double spectrographs fed by 640 fibers (Smee et al. 2013). The initial survey (York et al. 2000) carried out imaging in five broad bands (*ugriz*) (Fukugita et al. 1996) to a depth

[62] Alfred P. Sloan fellow.
[63] Institució Catalana de Recerca i Estudis Avançats, Barcelona E-08010, Spain.
[64] Institut de Ciències del Cosmos, Universitat de Barcelona/IEEC, Barcelona E-08028, Spain.
[65] US Naval Observatory, Flagstaff Station, 10391 West Naval Observatory Road, Flagstaff, AZ 86001-8521, USA.
[66] Department of Physics and Astronomy, University of Wyoming, Laramie, WY 82071, USA.
[67] Dunlap Institute for Astronomy and Astrophysics, University of Toronto, Toronto, ON, M5S 3H4, Canada.
[68] Dept. of Astronomy, University of Michigan, Ann Arbor, MI, 48104, USA.
[69] Departamento de Astronomía, Universidad de Chile, Casilla 36-D, Santiago, Chile.
[70] Department of Physics, Lehigh University, 16 Memorial Drive East, Bethlehem, PA 18015, USA.
[71] Departament d'Astronomia i Meteorologia, Facultat de Física, Universitat de Barcelona, E-08028 Barcelona, Spain.
[72] Federal do Rio de Janeiro, Observatório do Valongo, Ladeira do Pedro Antônio 43, 20080-090 Rio de Janeiro, Brazil.
[73] Campus of International Excellence UAM+CSIC, Cantoblanco, E-28049 Madrid, Spain.
[74] Instituto de Astrofísica de Andalucía (CSIC), Glorieta de la Astronomía, E-18080 Granada, Spain.
[75] Department of Astronomy, Columbia University, New York, NY 10027, USA.
[76] Consejo Superior Investigaciones Científicas, 28006 Madrid, Spain.
[77] Instituto de Física, UFRGS, Caixa Postal 15051, Porto Alegre, RS - 91501-970, Brazil.
[78] Université de Franche-Comté, Institut Utinam, UMR CNRS 6213, OSU Theta, Besançon, F-25010, France.
[79] UCO/Lick Observatory, University of California, Santa Cruz, 1156 High Street, Santa Cruz, CA 95064, USA.
[80] School of Physics, Korea Institute for Advanced Study, 85 Hoegiro, Dongdaemun-gu, Seoul 130-722, Republic of Korea.
[81] Astrophysics Research Institute, Liverpool John Moores University, IC2, Liverpool Science Park 146 Brownlow Hill Liverpool L3 5RF United Kingdom.
[82] Research School of Astronomy and Astrophysics, Australian National University, Weston Creek, ACT, 2611, Australia.
[83] Observatories of the Carnegie Institution of Washington, 813 Santa Barbara Street, Pasadena, CA 91101, USA.
[84] University of Texas, Hobby-Eberly Telescope, 32 Fowlkes Rd, McDonald Observatory, TX 79734-3005, USA.
[85] Brookhaven National Laboratory, Bldg 510, Upton, NY 11973, USA.
[86] Department of Astronomy and Astrophysics and JINA, University of Chicago, Chicago, IL 60637, USA.
[87] Department of Physics, Fisk University, 1000 17th Avenue North, Nashville, TN 37208, USA.
[88] Corresponding authors.
[89] Department of Astronomy, University of Wisconsin-Madison, 475 North Charter Street, Madison WI 53703, USA.
[90] Department of Physics, University of California, Berkeley, CA 94720, USA.
[91] Max-Planck Institute for Astrophysics, KarlSchwarzschildStr 1, D-85748 Garching, Germany.
[92] H.L. Dodge Department of Physics and Astronomy, University of Oklahoma, Norman, OK 73019, USA.
[93] PITT PACC, Department of Physics and Astronomy, University of Pittsburgh, Pittsburgh, PA 15260, USA.
[94] Department of Astronomy and Astrophysics and the Enrico Fermi Institute, University of Chicago, 5640 South Ellis Avenue, Chicago, IL 60637, USA.
[95] National Astronomy Observatories, Chinese Academy of

of $r \sim 22.5$ mag over 11,663 deg^2 of high-latitude sky, and spectroscopy of 1.6 million galaxy, quasar, and stellar targets over 9380 deg^2. The resulting images were calibrated astrometrically (Pier et al. 2003) and photometrically (Ivezić et al. 2004; Tucker et al. 2006; Padmanabhan et al. 2008), and the properties of the detected objects were measured (Lupton et al. 2001). The spectra were calibrated and redshifts and classifications determined (Bolton et al. 2012). The data have been released publicly in a series of roughly annual data releases (Stoughton et al. 2002; Abazajian et al. 2003, 2004, 2005; Adelman-McCarthy et al. 2006, 2007, 2008; Abazajian et al. 2009; hereafter EDR, DR1, DR2, DR3, DR4, DR5, DR6, DR7, respectively) as the project went through two funding phases, termed SDSS-I (2000–2005) and SDSS-II (2005–2008).

In 2008, the SDSS entered a new phase, designated SDSS-III (Eisenstein et al. 2011), in which it is currently operating. SDSS-III has four components. The Sloan Extension for Galactic Understanding and Exploration 2 (SEGUE-2), an expansion of a similar project carried out in SDSS-II (Yanny et al. 2009), used the SDSS spectrographs to obtain spectra of about 119,000 stars, mostly at high Galactic latitudes. The Baryon Oscillation Spectroscopic Survey (BOSS; Dawson et al. 2013) rebuilt the spectrographs to improve throughput and increase the number of fibers to 1000 (Smee et al. 2013). BOSS enlarged the imaging footprint of SDSS to 14,555 deg^2, and is obtaining spectra of galaxies and quasars with the primary goal of measuring the oscillation signature in the clustering of matter as a cosmic yardstick to constrain cosmological models. The Multi-Object APO Radial Velocity Exoplanet Large-area Survey (MARVELS), which finished its data-taking in 2012, used a 60-fiber interferometric spectrograph to measure high-precision radial velocities of stars in a search for planets and brown dwarfs. Finally, the Apache Point Observatory Galactic Evolution Experiment (APOGEE) uses a 300-fiber spectrograph to observe bright ($H < 13.8$ mag) stars in the H band at high resolution ($R \sim 22,500$) for accurate radial velocities and detailed elemental abundance determinations.

We have previously had two public data releases of data from SDSS-III. The Eighth Data Release (DR8; Aihara et al. 2011) included all data from the SEGUE-2 survey, as well as ~ 2500 deg^2 of new imaging data in the Southern Galactic Cap as part of BOSS. The Ninth Data Release (DR9, Ahn et al. 2012) included the first spectroscopic data from the BOSS survey: over 800,000 spectra selected from 3275 deg^2 of sky.

This paper describes the Tenth Data Release (hereafter DR10) of the SDSS survey. This release includes almost 680,000 new BOSS spectra, covering an additional 3100 deg^2 of sky. It also includes the first public release of APOGEE spectra, with almost 180,000 spectra of more than 57,000 stars in a wide range of Galactic environments. As in previous SDSS data releases, DR10 is cumulative; it includes all data that were part of DR1–9. All data released with DR10 are publicly available on the SDSS-III website[96] and links from it.

Science, Beijing, 100012, China.
[96] http://www.sdss3.org/dr10/

The scope of the data release is described in detail in Section 2. We describe the APOGEE data in Section 3, and the new BOSS data in Section 4. The mechanisms for data access are described in Section 5. We outline the future of SDSS in Section 6.

2. SCOPE OF DR10

DR10 presents the release of the first year of data from the SDSS-III APOGEE infrared spectroscopic survey and the first 2.5 years of data from the SDSS-III BOSS optical spectroscopic survey. In each case these data extend to the 2012 telescope shutdown for the summer monsoon season.

APOGEE was commissioned from 2011 May up through the summer shutdown in 2011 July. Survey-quality observations began 2011 Aug 31 (UTC-7), corresponding to Modified Julian Date (MJD) 55804. The APOGEE data presented in DR10 include all commissioning and survey data taken up to and including MJD 56121 (2012 July 13). However, detailed stellar parameters are only presented for APOGEE spectra obtained after commissioning was complete. The BOSS data include all data taken up to and including MJD 56107 (2012 June 29).

DR10 also includes the imaging and spectroscopic data from SDSS-I/II and SDSS-III SEGUE-2, the imaging data for the BOSS Southern Galactic Cap first presented in DR8, as well as the spectroscopy from the first 2.5 years of BOSS. Table 1 lists the contents of the data release, including the imaging coverage and number of APOGEE and BOSS plates and spectra. APOGEE plates are observed multiple times ("visits") to build signal-to-noise ratio (S/N) and to search for radial velocity variations; thus the number of spectra in DR10 is significantly larger than the number of unique stars observed. While there are fewer repeat spectra in BOSS, we sill distinguish between the total number of spectra, and the number of unique objects observed in BOSS as well. The numbers for the imaging data, unchanged since DR8, also distinguish between unique and total area and number of detected objects. The multiple repeat observations of the Equatorial Stripe in the Fall sky (Annis et al. 2011), used to search for Type Ia supernovae (Frieman et al. 2008), dominate the difference between total and unique area imaged.

New in DR10 are morphological classifications of SDSS images of galaxies by 200,000 citizen scientists via the Galaxy Zoo project (Lintott et al. 2008, 2011; Willett et al. 2013). These classifications include both the basic (spiral–early-type) morphologies for all ∼1 million galaxies from the SDSS-I/II Main Galaxy Sample (Strauss et al. 2002), as well as more detailed classifications of the internal structures in the brightest 250,000 galaxies.

The celestial footprint of the APOGEE spectroscopic coverage in DR10 is shown in Figure 1 in Galactic coordinates; Figure 2 repeats this in Equatorial coordinates, and shows the imaging and BOSS spectroscopy sky coverage as well. The distribution on the sky of SDSS-I/II and SEGUE-2 spectroscopy is not shown here; see the DR7 and DR8 papers. APOGEE fields span all of the Galactic components visible from APO, including the Galactic center and disk, as well as fields at high Galactic latitudes to probe the halo. The Galactic center observations occur at high airmass, thus the differential atmo-

spheric refraction across the field of view changes rapidly with hour angle. Therefore targets in these fields are not distributed over the full 7 deg^2 of each plate, but rather over a smaller region from 0.8 to 3.1 deg^2, as indicated by the smaller dots in Figure 1. The clump of points centered roughly at $l = 75°, b = +15°$ are special plates targeting stars previously observed by NASA's *Kepler* mission, as described in detail in Section 3.4.

The additional BOSS spectroscopy fills in most of the "doughnut" defined by the DR9 coverage in the North Galactic Cap. The DR10 BOSS sky coverage relative to the 10,000 deg^2 full survey region is described further in Section 4.

3. THE APACHE POINT OBSERVATORY GALAXY EVOLUTION EXPERIMENT (APOGEE)

3.1. *Overview of APOGEE*

Stellar spectra of red giants in the H band (1.5–1.8 μm) show a rich range of absorption lines from a wide variety of elements. At these wavelengths, the absorption due to dust in the plane of the Milky Way is much reduced compared to that in the optical bands. A high-resolution study of stars in the H band allows studies of all components of the Milky Way, across the disk, in the bulge, and out to the halo.

APOGEE's goal is to trace the history of star formation in, and the assembly of, the Milky Way by obtaining H-band spectra of 100,000 red giant candidate stars throughout the Galaxy. Using an infrared multi-object spectrograph with a resolution of $R \equiv \lambda/\Delta\lambda \sim 22,500$, APOGEE can survey the halo, disk, and bulge in a much more uniform fashion than previous surveys. The APOGEE spectrograph features a 50.8 cm × 30.5 cm mosaiced volume-phase holographic (VPH) grating and a six-element camera having lenses with a maximum diameter of 40 cm. APOGEE takes advantage of the fiber infrastructure on the SDSS telescope, using 300 fibers, each subtending 2″ on the sky, distributed over the full 7 deg^2 field of view (with the exception of plates observed at high airmass, as noted above). The spectrograph itself sits in a temperature-controlled room, and thus does not move with the telescope. The light from the fibers falls onto three HAWAII-2RG 2K × 2K infrared detectors (Garnett et al. 2004; Rieke 2007), that cover the wavelength range from 1.514 μm to 1.696 μm, with two gaps (see Section 3.2 for details). APOGEE targets are chosen with magnitude and color cuts from photometry of the Two-Micron All-Sky Survey (2MASS; Skrutskie et al. 2006), with a median $H = 10.9$ mag and with 99.6% of the stars brighter than $H = 13.8$ mag (on the 2MASS Vega-based system).

The high resolution of the spectra and the stability of the instrument allow accurate radial velocities with a typical uncertainty of $100\,\mathrm{m\,s^{-1}}$, and detailed abundance determinations for approximately 15 chemical elements. In addition to being key in identifying binary star systems, the radial velocity data are being used to explore the kinematical structure of the Milky Way and its substructures (e.g., Nidever et al. 2012) and to constrain dynamical models of its disk (e.g., Bovy et al. 2012). The chemical abundance data allow studies of the chemical evolution of the Galaxy (García Pérez et al. 2013) and the history of star formation. The combination of kinematical and chemical data will allow important new
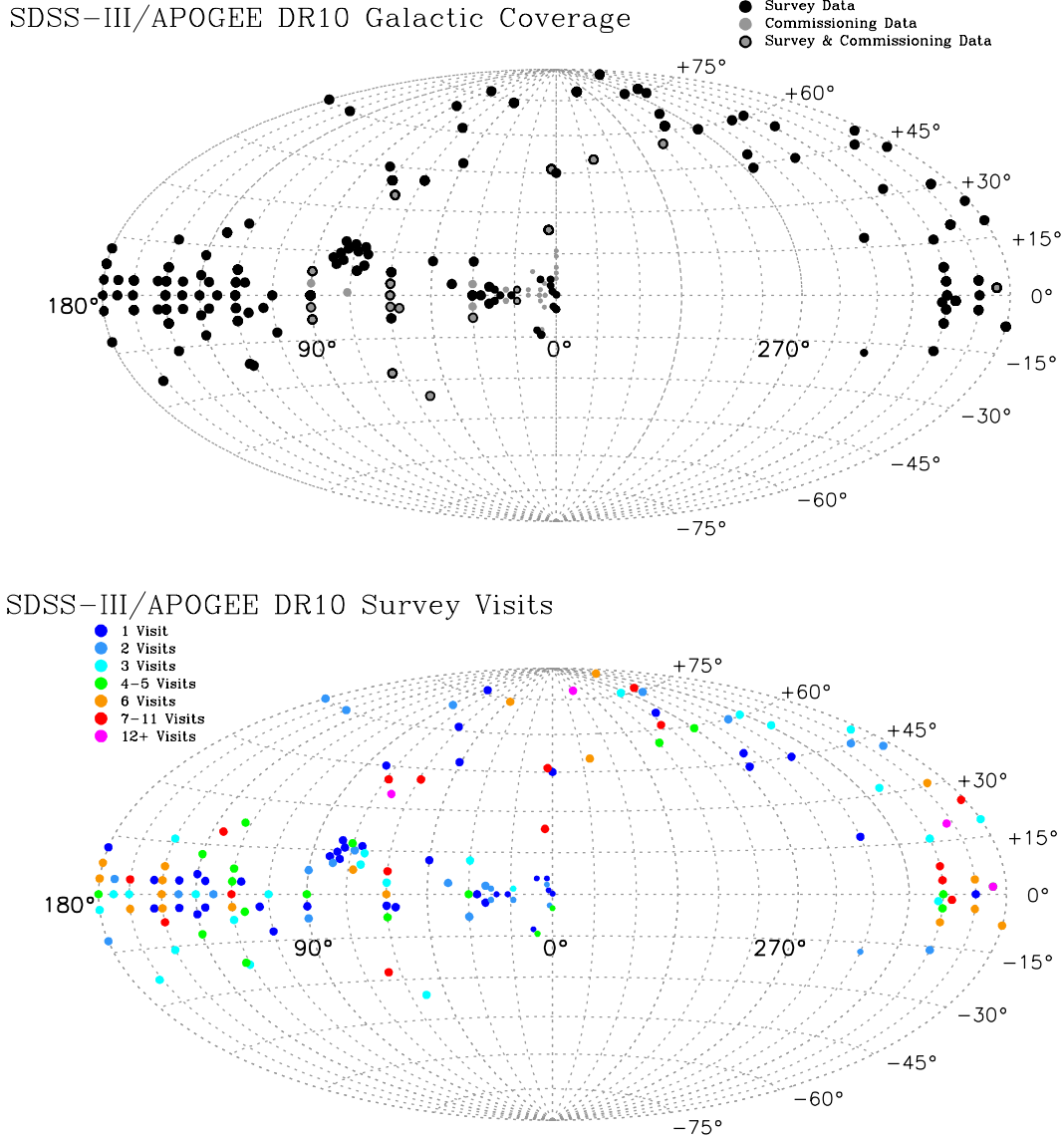
SDSS−III/APOGEE DR10 Galactic Coverage

SDSS−III/APOGEE DR10 Survey Visits

Figure 1. The distribution on the sky of all APOGEE DR10 pointings in Galactic coordinates: the Galactic Center is in the middle of the diagram. Each circle represents a pointing. APOGEE often has several distinct plates for a single location on the sky; DR10 includes 170 locations, which are shown above. Smaller circles (primarily near the Galactic Center) represent locations where plates were drilled over only a fraction of the 7 deg^2 focal plane to minimize differential atmospheric refraction. Note the concentration of fields along the Galactic Plane. The concentration of pointings at $l = 75°, b = +15°$ is a special program targeting stars observed by the *Kepler* telescope; see Section 3.4. (top) Distribution of pointings in both the commissioning and survey phases (both are included in DR10). (bottom) Pointings distinguished by the number of visits obtained by DR10 in the survey phase.

constraints on the formation history of the Milky Way.

A full overview of the APOGEE survey will be presented in S. Majewski et al. (2014, in preparation). The APOGEE instrument will be detailed in J. Wilson et al. (2014, in preparation) and is summarized here in Section 3.2. The target selection process for APOGEE is described in Zasowski et al. (2013) and is presented in brief here in Section 3.3. In Section 3.4 we describe a unique cross-targeting program between SDSS-III APOGEE and asteroseismology measurements from the NASA *Kepler* telescope[97] (Gilliland et al. 2010). Section 3.5 describes the reduction pipeline that pro-

cesses the APOGEE data and produces calibrated one-dimensional spectra of each star, including accurate radial velocities (D. Nidever et al., 2014, in preparation). Important caveats regarding APOGEE data of which potential users should be aware are described in Section 3.6. Section 3.7 describes the pipeline that measures stellar properties and elemental abundances – the APOGEE Stellar Parameters and Chemical Abundances Pipeline (ASPCAP; M. Shetrone et al., 2014, in preparation; A. García-Pérez et al., 2014, in preparation, Mészáros et al. 2013). Section 3.8 summarizes the APOGEE data products available in DR10.
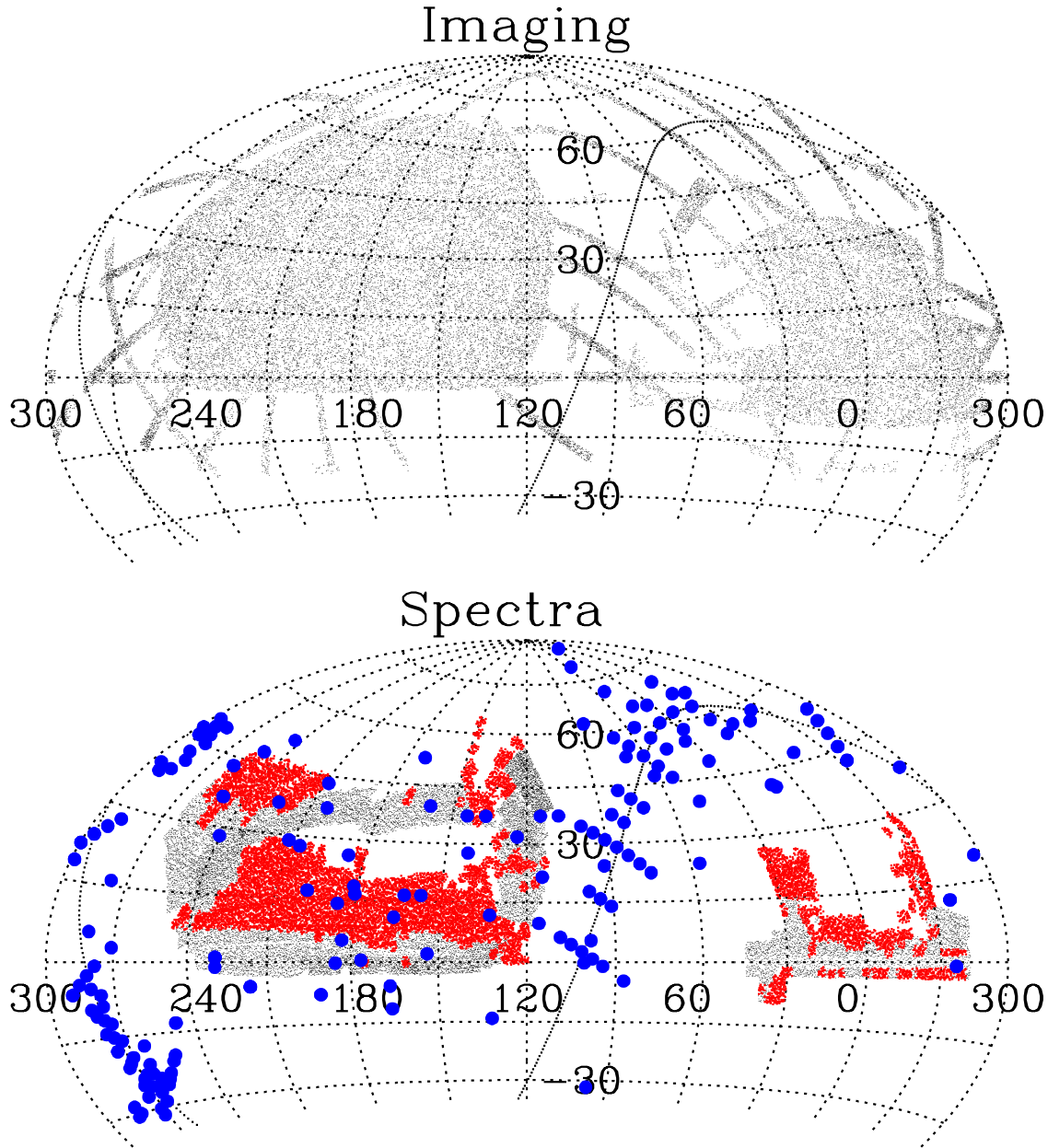
3.2. The APOGEE Instrument and Observations

Imaging

Spectra

Figure 2. The distribution on the sky of all SDSS imaging (top; 14,555 deg^2 – same as DR8 and DR9) and BOSS and APOGEE DR10 spectroscopy (bottom; 6373.2 deg^2) in J2000 equatorial coordinates ($\alpha = 0°$ is right of center in this projection). Grey shows regions included in DR9; the increment included in DR10 is in red. The blue shows the positions of APOGEE pointings included in DR10. The Galactic Plane is shown by the dotted line. The Northern Galactic Cap is on the left of the figure, and the Southern Galactic Cap on the right. The BOSS sky coverage shown is actually constructed using a random subsample of the BOSS DR10Q quasar catalog (Pâris et al. 2013). The sky below $\delta < -30°$ is never at an airmass of of less than 2.0 from APO (latitude=+32°46′49″).

The APOGEE spectrograph measures 300 spectra in a single observation: roughly 230 science targets, 35 on blank areas of sky to measure sky emission, and 35 hot, blue stars to calibrate atmospheric absorption. This multiplexing is accomplished using the same aluminum plates and fiber optic technology as have been used for the optical spectrograph surveys of SDSS. Each plate corresponds to a specific patch of sky, and is pre-drilled with holes corresponding to the sky positions of objects in that area, meaning that each area requires one or more unique plates.

The APOGEE spectrograph uses three detectors to cover the H-band range, "blue": 1.514–1.581 μm, "green": 1.585–1.644 μm, and "red": 1.647–1.696 μm. There are two gaps, each a few nm wide, in wavelength in the spectra. The spectral line spread function spans 1.6–3.2 pixels per spectral resolution element FWHM, increasing from blue to red across the detectors. Thus most of the blue detector is under-sampled. Figure 3 shows the results of a typical exposure. Each observation consists of at least one "AB" pair of exposures for a given pointing on the sky, with the detector array mechanically offset by 0.5 pixels along the dispersion direction between the two exposures. This well-controlled sub-pixel dithering
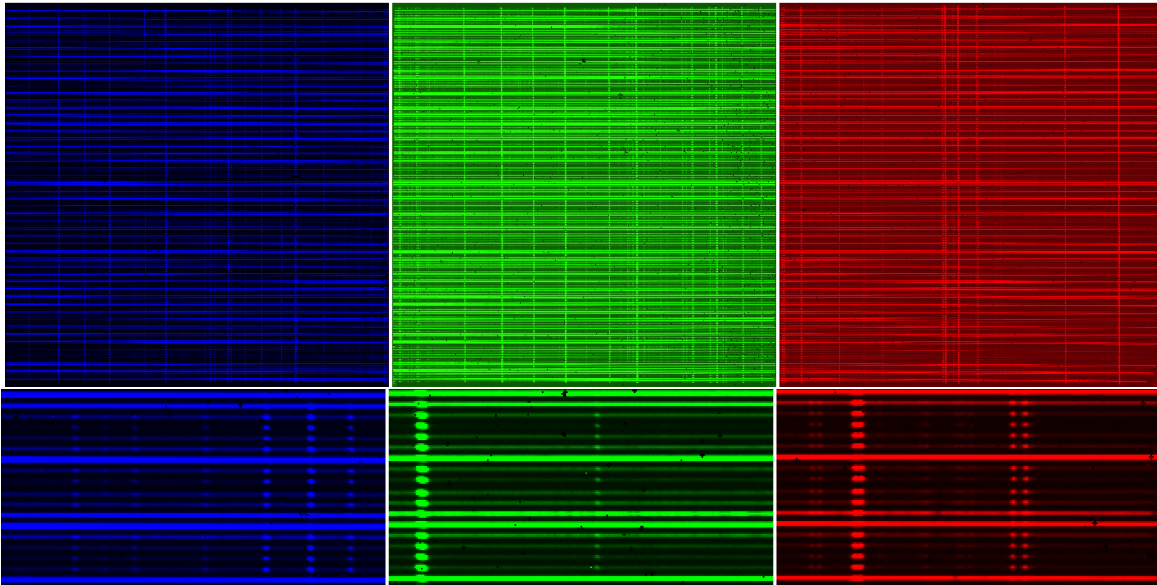
Figure 3. (top) A 2D spectrogram from the APOGEE instrument. The three chips ("blue", "green", and "red") are shown with wavelength increasing to the right across the full APOGEE wavelength range of 1.514–1.696 μm. The gaps between the chips are slightly larger than as displayed in this image. Each fiber is imaged onto several pixels (vertically). Note the vertical series of points from sky lines in each fiber, and the horizontal spectra of faint stars and sky fibers. (bottom) Expanded view of the central 18 fibers and central 6 nm of each chip.

allows the derivation of combined spectra with approximately twice the sampling of the individual exposures. Thus the combined spectra are properly sampled, including all wavelengths from the blue detector. The actual line spread function as a function of wavelength is provided as a Gauss-Hermite function for each APOGEE spectrum in DR10.

A typical observation strategy is two "ABBA" sequences. Each sequence consists of four 500-second exposures to reach the target S/N for a given observation. The combination of all "AB" or "BA" pairs for a given plate during a night is called a "visit." The visit is the basic product for what are considered individual spectra for APOGEE (although the spectra from the individual exposures are also made available). While the total exposure time for a visit is 4,000 seconds ($2 \times 4 \times 500$ seconds), due to the varying lengths of night and other scheduling issues, we often gathered more or less than the standard two "ABBA" sequences on a given plate in a night. APOGEE stars are observed over multiple visits (the goal is at least three visits) to achieve the planned S/N. Figure 4 shows the distribution of the number of visits for stars included in DR10; presently, most stars have three or fewer visits, but this distribution will broaden with the final data release. These visits are separated across different nights and often different seasons, allowing us to look for radial velocity variability due to binarity on a variety of timescales. The distribution of time intervals between visits is shown in Figure 5, with peaks at one and two lunations (30 and 60 days).

Each visit is uniquely identified by the plate number and MJD of the observation. Plates are generally re-plugged between observations, so while "plate+MJD+fiber" remains a unique identifier in APOGEE spectra as it is in optical SDSS spectra, "plate+fiber" does not refer to the same object across all visits. The spectra from all visits are co-added to produce the aggregate spectrum of the star. The final
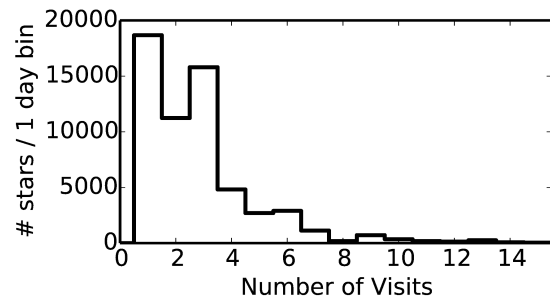

Figure 4. The distribution of number of spectroscopic visits for APOGEE stars included in DR10. While the bulk of stars have three or fewer visits, they may have reached our spectral S/N requirement if they are bright enough; see Figure 7.

co-added spectra are processed by the stellar parameters pipeline described in Section 3.7.

The aim is for a final co-added spectrum of each star with a S/N of > 100 per half-resolution element.[98] Figures 6 and 7 show the distribution of S/N; not surprisingly, S/N is strongly correlated with the brightness of the star. The DR10 data include some stars that have yet to receive their full complement of visits and thus have significantly lower quality spectra. Future data releases will include additional visits for many stars, leading to an increase in total co-added S/N as well as more refined stellar parameters.

The APOGEE plates are drilled with the same plate-drilling machines used for BOSS, and the plate numbers are sequential. This scheme means that the BOSS and APOGEE plate numbers are interleaved and that no plate number is assigned to both a BOSS and APOGEE plate.

The quality of the APOGEE commissioning data (that taken prior to 2011 Aug 31) is lower than the survey data,

---

[98] This is a refinement from the less stringent goal of S/N> 100 per full-resolution element given in Eisenstein et al. (2011).

Table 1
Contents of DR10

Optical Imaging[a]		
	Total	Unique[b]
Area Imaged [deg^2]	31637	14555
Cataloged Objects	1231051050	469053874

APOGEE Spectroscopy			
	Commiss.	Survey	Total
Plate-Visits	98	586	684
Plates	51	232	281
Pointings	43	150	170
		Spectra	Stars
All Stars[c]		178397	57454
Commissioning Stars		24943	11987
Survey Stars		153454	47452
Stars with S/N > 100[d]		$\cdots$	47675
Stars with $\geq$ 3 visits		$\cdots$	29701
Stars with $\geq$ 12 visits		$\cdots$	923
Stellar parameter standards		5178	1065
Radial velocity standards		162	16
Telluric line standards		24283	7003
Ancillary science program objects		8894	3344

BOSS Spectroscopy		
	Total	Unique[b]
Spectroscopic effective area [deg^2]	$\cdots$	6373.2
Plates[e]	1515	1489
Optical Spectra observed[f]	1507954	1391792
All Galaxies	927844	859322
CMASS[g]	612195	565631
LOWZ[g]	224172	208933
All Quasars	182009	166300
Main[h]	159808	147242
Main, $2.15 < z < 3.5$[i]	114977	105489
Ancillary program spectra	72184	65494
Stars	159327	144968
Standard stars	30514	27003
Sky spectra	144503	138491
Unclassified spectra[j]	101550	89003

All Optical Spectroscopy from SDSS up through DR10	
Total spectra	3358200
Total useful spectra[k]	3276914
Galaxies	1848851
Quasars	316125
Stars	736484
Sky	247549
Unclassified[j]	138663

[a] These numbers are unchanged since DR8.
[b] Removing all duplicates, overlaps, and repeat visits from the "Total" column.
[c] 2,155 stars were observed both during the commissioning and survey phases. The co-added spectra are kept separate between these two phases. Thus the number of coadded spectra is greater than the number of unique stars observed.
[d] Signal-to-noise ratio per half resolution element > 100.
[e] Twenty-six plates of the 1515 observed plates were re-plugged and re-observed for calibration purposes. Six of the 1489 unique plates are different drillings of the same set of objects.
[f] This excludes the small fraction of the observations through fibers that are broken or that fell out of their holes after plugging. There were 1,515,000 spectra attempted.
[g] "CMASS" and "LOWZ" refer to the two galaxy target categories used in BOSS (Ahn et al. 2012). They are both color-selected, with LOWZ galaxies in the redshift range $0.15 < z < 0.4$, and CMASS galaxies in the range $0.4 < z < 0.8$.
[h] This counts only quasars that were targeted by the main quasar survey (Ross et al. 2012), and thus does not include those from ancillary programs (Dawson et al. 2013).
[i] Quasars with redshifts in the range $2.15 < z < 3.5$ provide the most signal in the BOSS spectra of the Ly-α forest.
[j] Non-sky spectra for which the automated redshift/classification pipeline (Bolton et al. 2012) gave no reliable classification, as indicated by the ZWARNING flag.
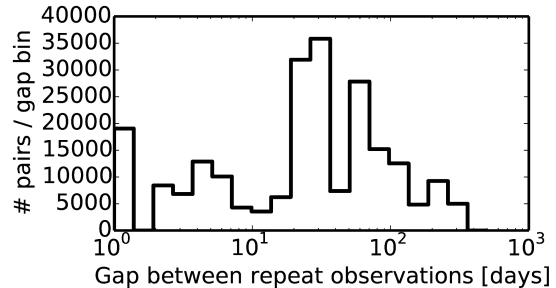[k] Spectra on good or marginal plates.

Figure 5. The distribution of time between visits for APOGEE stars, useful for determining the sensitivity to radial velocity variations due to binarity. This quantity is the absolute value of the time difference for all unique pairs of visits for each star. The most prominent peaks are at one and two months.
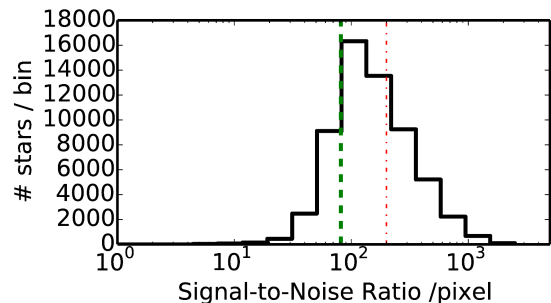

Figure 6. Reported S/N per pixel of APOGEE DR10 co-added stellar spectra. Repeated observations imply that there is a practical limit of S/N $\sim$ 200 in the co-added spectra, shown as the dot-dashed line. The dashed line denotes the goal of S/N $\sim$ 100 per half-resolution element, corresponding to S/N $\sim$ 80 per pixel in the co-added spectra.
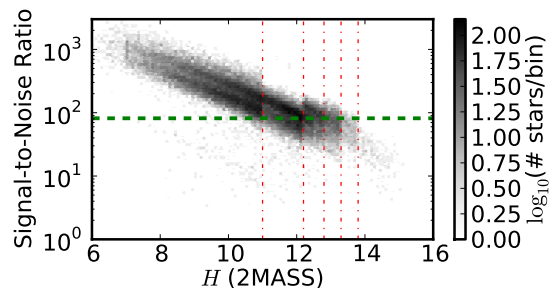

Figure 7. S/N per pixel of spectra of stars as a function of their apparent H-band magnitude (density is on a log scale). The vertical dot-dashed lines indicate the magnitude limits for stars at each value of the final number of visits: 1, 3, 6, 12, 24 visits for $H = 11.0$, 12.2, 12.8, 13.3, and 13.8 mag. The horizontal dashed line denotes the target S/N $\sim$ 100 per half-resolution element, corresponding to S/N $\sim$ 80 per pixel in the co-added spectra.

due to optical distortions and focus issues that were resolved before the official survey was started. The biggest difference lies in the "red" chip, which has significantly worse spectral resolution in the commissioning data than in the survey data. Because of this degradation, the data were not under-sampled, and spectral dithering was not done during commissioning.

Many of the targets observed in commissioning were selected in the same way as those observed during the survey (Section 3.3), though several test plates were designed with different criteria to test the selection algorithms (e.g., without a color limit or with large numbers of potential telluric calibration stars). Total exposure

times for the commissioning plates were similar to those of the survey plates. Because the spectral resolution of commissioning data is worse, it cannot be analyzed using ASPCAP with the same spectral libraries with which the survey data are analyzed. As a result, DR10 does not release any stellar parameters other than radial velocities for commissioning data; subsequent releases may include stellar parameters for APOGEE commissioning derived using appropriately matched libraries and/or with only a subset of the spectral range.

3.3. APOGEE Main and Ancillary Targets

APOGEE main targets are selected from 2MASS data (Skrutskie et al. 2006) using apparent magnitude limits to meet the S/N goals and a dereddened color cut of $(J - K_s)_0 > 0.5$ mag to select red giants in multiple components of the Galaxy: the disk, bulge, and halo. This selection results in a sample of objects that are predominantly red giant stars with $3500 < T_{\rm eff} < 5200$ K and $\log g < 3.5$ (where g is in cm s^{-2} and the logarithm is base 10). Fields receiving three visits have a magnitude limit of $H = 12.2$; the deepest plates with 24 visits go to $H = 13.8$.

APOGEE has also implemented a number of ancillary programs to pursue specific investigations enabled by its unique instrument. The selection of the main target sample and the ancillary programs, together with the bit flags that can be used to identify why an object was targeted for spectroscopy, are described in detail in Zasowski et al. (2013). In DR10, APOGEE stars are named based on a slightly shortened version of their 2MASS ID (e.g., "2M21504373+4215257" is stored for the formal designation "2MASS 21504373+4215257"). A few objects that don't have 2MASS IDs are designated as "AP", followed by their coordinates.

APOGEE targets were chosen in a series of fields designed to sample a wide range of Galactic environments (Figure 1): in the halo predominantly at high latitudes, in the disk, in the central part of the Milky Way (limited in declination), as well as special targeted fields overlapping the Kepler survey (Section 3.4), and a variety of open and globular clusters with well-characterized metallicity in the literature.

The effects of Galactic extinction on 2MASS photometry can be quite significant at low Galactic latitude. We correct for this using the *Spitzer* IRAC GLIMPSE survey (Benjamin et al. 2003; Churchwell et al. 2009) and the Wide-field Infrared Survey Explorer (WISE; Wright et al. 2010) $\lambda = 4.5$ μm data following the Rayleigh-Jeans Color Excess Method described in Majewski et al. (2011) and Zasowski et al. (2013) using the color extinction curve from Indebetouw et al. (2005). Figure 8 shows the measured and reddening-corrected JHK_s color-color and magnitude-color diagrams for the APOGEE stars included in DR10.

In regions of high interstellar extinction, even intrinsically blue main sequence stars can be reddened enough to overlap the nominal red giant locus. Dereddening these apparent colors allows us to remove these dwarfs with high efficiency from the final targeted sample. However, G and K dwarfs cannot be distinguished from red giants on the basis of their dereddened broadband colors, with the result that a fraction of the APOGEE sample is composed of such dwarfs. In the disk they are expected to
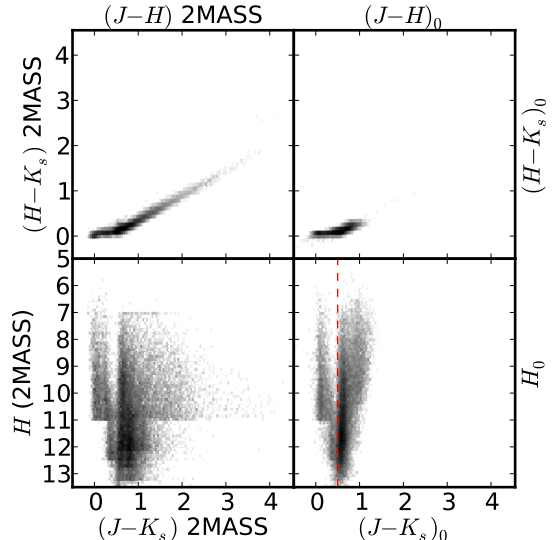

Figure 8. Two-dimensional histogram of the APOGEE DR10 stars in (top) 2MASS JHK_s color space; and (bottom) 2MASS H vs. $J - K_s$. The left column shows observed magnitudes and colors from 2MASS, while the right column has been dereddened based on $H - 4.5$ μm color as in Zasowski et al. (2013). The vertical dashed line at $(J - K_s)_0 = 0.5$ shows the selection of the main APOGEE red giant sample; bluer objects include telluric calibration stars, data taken during commissioning, and ancillary program targets. The grey scale is logarithmic in number of stars.

comprise less than 20% of the sample, and this appears to be validated by our analysis of the spectra. Disk dwarfs are expected to be a larger contaminant in halo fields, so in many of these, target selection was supplemented by Washington and intermediate-band DDO51 photometry (Canterna 1976; Clark & McClure 1979; Majewski et al. 2000) using the 1.3-m telescope of the U.S. Naval Observatory, Flagstaff Station. Combining this with 2MASS photometry allows us to distinguish dwarfs and giants (see Zasowski et al. 2013 for details).

Exceptions to the $(J - K_s)_0 > 0.5$ mag color limit that appear in DR10 include the telluric calibration stars, early-type stars targeted in well-studied open clusters, stars observed on commissioning plates that did not employ the color limit, and stars in sparsely populated halo fields where a bluer color limit of $(J - K_s)_0 > 0.3$ mag was employed to ensure that all fibers were utilized. Ancillary program targets may also have colors and magnitudes beyond the limits of APOGEE's normal red giant sample.

3.4. APOKASC

Non-radial oscillations are detected in virtually all red giants targeted by the *Kepler* mission (Borucki et al. 2010; Hekker et al. 2011), and the observed frequencies are sensitive diagnostics of basic stellar properties such as mass, radius, and age (for a review, see Chaplin & Miglio 2013). Abundances and surface gravities measured from high-resolution spectroscopy of these same stars are an important test of stellar evolution models, and allow observational degeneracies to be broken.

With this in mind, the "APOKASC" collaboration was formed between SDSS-III and the *Kepler* Asteroseismology Science Collaboration (KASC) to analyze APOGEE spectra for $\sim 10,000$ stars in fields observed by the *Kepler* telescope (see Figure 1). The joint measurement

of masses, radii, ages, evolutionary states, and chemical abundances for all these stars will enable significantly enhanced investigations of Galactic stellar populations and fundamental stellar physics.

DR10 presents 4,204 spectra of 2,308 stars of the anticipated final APOKASC sample. Asteroseismic data from the APOKASC collaboration were used to calibrate the APOGEE spectroscopic surface gravity results for all APOGEE stars presented in DR10 (Mészáros et al. 2013). A joint asteroseismic and spectroscopic value-added catalog will be released separately (M. Pinsonneault et al., 2014, in preparation).

3.5. APOGEE Data Analysis

The processing of the two-dimensional spectrograms and extraction of one-dimensional co-added spectra will be fully described in D. Nidever et al. (2014, in preparation). We provide here a brief summary to help the reader understand how individual APOGEE exposures are processed. A 500-second APOGEE exposure actually consists of a series of non-destructive readouts every 10.7 seconds that result in a three-dimensional data cube. The first step in processing is to extract a two-dimensional image from a combination of these measurements. After dark current subtraction, the "up-the-ramp" values for each pixel are fit to a line to derive the count rate for that pixel. Cosmic rays create characteristic jumps in the "up-the-ramp" signal that are easily recognized, removed, and flagged for future reference. The count rate in each pixel is multiplied by the exposure time to obtain a two-dimensional image. These two-dimensional images are then dark-subtracted and flat-fielded. One-dimensional spectra are extracted simultaneously for the entire set of 300 fibers based on wavelength and profile fits from flat-field calibration images. Both the flat-field response and spectral traces are very stable due to the controlled environment of the APOGEE instrument, which has been under vacuum and at a uniform temperature continuously since it was commissioned. Wavelength calibration is performed using emission lines from thorium-argon and uranium-neon hollow cathode lamps. The wavelength solution is then adjusted from the reference lamp calibration on an exposure-to-exposure basis using the location of the night sky lines.

The individual exposure spectra are then corrected for telluric absorption and sky emission using the sky spectra and telluric calibration star spectra, and combined accounting for the dither offset between each "A" and "B" exposure. This combined visit spectrum is flux-calibrated based on a model of the APOGEE instrument's response from observations of a blackbody source. The spectrum is then scaled to match the 2MASS measured apparent H-band magnitude. A preliminary radial velocity is measured after matching the visit spectrum to one from a pre-computed grid of synthetic stellar spectra, and is stored with the individual visit spectrum.

In addition to the individual visit spectra, the APOGEE software pipeline coadds the spectra from different visits to the same field, yielding a higher S/N spectrum of each object. Figure 9 shows examples of high S/N co-added flux-calibrated spectra from APOGEE for stars with a range of $T_{\rm eff}$ and with a range of [M/H]. A final and precise determination of the relative radial velocities on each visit is determined from cross-correlation of each visit spectrum with the combined spectrum; the velocities are put on an absolute scale by cross-correlating the combined spectrum with the best-matching spectrum in a pre-computed synthetic grid. The combined spectra are output on a rest-wavelength scale with logarithmically spaced pixels with approximately three pixels per spectral resolution element.

3.6. Issues with APOGEE Spectra

Users should be aware of several features and potential issues with the APOGEE data. This is the first data release for APOGEE; the handling of some of these issues by the pipelines may be improved in subsequent data releases.

Many of these issues are documented in the data by the use of bitmasks that flag various conditions. For the APOGEE spectral data, there are two bitmasks that accompany the main data products Each one-dimensional extracted spectrum includes a signal, uncertainty, and mask arrays. The mask array is a bitmask, APOGEE_PIXMASK[99], that flags data-quality conditions that affect a given pixel. A non-zero APOGEE_PIXMASK value for a pixel indicates a potential data-quality concern that affects that pixel. Each stellar-parameters analysis of each star is accompanied by a single bitmask, APOGEE_STARFLAG[100], that flags conditions at the full spectrum level.

The most important data-quality features to be aware of include:

Gaps in the spectra: There are gaps in the spectra corresponding to the regions that fall between the three detectors. There are additional gaps due to bad or hot pixels on the arrays. As multiple dithered exposures are combined to make a visit spectrum, values from missing regions cannot be used to calculate the dither-combined signal in nearby pixels; as a result, these nearby pixels are set to zero and the BADPIX bit is set for these pixels in APOGEE_PIXMASK. Generally, the bad pixels affect neighboring pixels only at a very low level, and the data in the latter may be usable; in subsequent data releases, we will preserve more of the data, while continuing to identify potential bad pixels in the pixel mask.

Imperfect night-sky-line subtraction: The Earth's atmosphere has strong and variable emission in OH lines in the APOGEE bandpass. At the location of these lines, the sky flux is many times brighter than the stellar flux for all except the brightest stars. Even if the sky subtraction algorithm were perfect, the photon noise at the positions of these sky lines would dominate the signal, so there is little useful information at the corresponding wavelengths. The spectra in these regions can show significant sky line residuals. These regions are masked for the stellar parameter analysis so that they do not impact the results. The affected pixels have the SIG_SKYLINE bit set in APOGEE_PIXMASK.

Error arrays do not track correlated errors: APOGEE spectra from an individual visit are made by combining multiple individual exposures taken at different dither positions. Because the dithers are not spaced by *exactly* 0.5 pixels, there is some correlation between

---

[99] http://www.sdss3.org/dr10/algorithms/bitmask_apogee_pixmask.php
[100] http://www.sdss3.org/dr10/algorithms/bitmask_apogee_starflag.php

pixels that is introduced when combined spectra are produced. The error arrays for the visit spectra do not include information about these correlations. In the visit spectra, these correlations are generally small because the dither mechanism is generally quite accurate. However, when multiple visit spectra are combined to make the final combined spectra, they must be re-sampled onto a common wavelength grid, taking into account the different observer-frame velocities of each individual visit. This re-sampling introduces significant additional correlated errors between adjacent pixels that are also not tracked in the error arrays.

Error arrays do not include systematic error floors: The errors that are reported for each spectrum are derived based on propagation of Poisson and readout noise. However, based on observations of bright hot stars, we believe that other, possibly systematic, uncertainties currently limit APOGEE observations to a maximum S/N per half resolution element of ~ 200. The error arrays published in DR10 currently report the estimated errors without any contribution from a systematic component. However, for the ASPCAP analysis, we impose an error floor corresponding to 0.5% of the continuum level.

Fiber crosstalk: While an effort is made not to put faint stars adjacent to bright ones on the detector to avoid excessive spillage of light from one to the other, this occasionally occurs. We flag objects (in APOGEE_STARFLAG) with a BRIGHT_NEIGHBOR flag if an adjacent star is > 10 times brighter than the object, and with a VERY_BRIGHT_NEIGHBOR flag if an adjacent star is > 100 times brighter; in the latter case, the individual spectra are marked as bad and are not used in combined spectra.

Persistence in the "blue" chip: There is a known "superpersistence" in 1/3 of the region of the "blue" APOGEE data array, and to a lesser extent in some regions of the "green" chip, whereby some of the charge from previous exposures persists in subsequent exposures. Thus the values read out in these locations depend on the previous exposure history for that chip. The effect of superpersistence can vary significantly, but residual signal can amount to as much as 10–20% of the signal from previous exposures. The current pipeline does not attempt to correct for this effect; any such correction is likely to be rather complex. For the current release, pixels known to be affected by persistence are flagged in APOGEE_PIXMASK at three different levels (PERSIST_LOW, PERSIST_MEDIUM, PERSIST_HIGH). Spectra that have significant numbers of pixels ($> 20\%$ of total pixels) that fall in the persistence region have comparable bits set in the APOGEE_STARFLAG bitmask to warn that the spectra for these objects may be contaminated. In a few cases, the effect of persistence is seen dramatically as an elevated number of counts in the blue chip relative to the other arrays; these are flagged as PERSIST_JUMP_POS in APOGEE_STARFLAG. We are still actively investigating the effect of persistence on APOGEE spectra and derived stellar parameters, and are working on corrections that we intend to implement for future data releases.

3.7. APOGEE Stellar Parameter and Chemical Abundances Pipeline (ASPCAP)

The ultimate goal of APOGEE is to determine the effective temperature, surface gravity, overall metallicity, and detailed chemical abundances for a large sample of stars in the Milky Way. Stellar parameters and chemical abundances are extracted from the continuum-normalized co-added APOGEE spectra by comparing with synthetic spectra calculated using state-of-the-art model photospheres (Mészáros et al. 2012) and atomic and molecular line opacities (Shetrone et al., in preparation).

Analysis of high-resolution spectra is traditionally done by hand. However, given the sheer size of APOGEE's spectral database, automatic analysis methods must be implemented. For that purpose, ASPCAP searches for the best fitting spectrum through χ^2 minimization within a pre-computed multi-dimensional grid of synthetic spectra, allowing for interpolation within the grid. The output parameters of the analysis are effective temperature ($T_{\rm eff}$), surface gravity ($\log g$), metallicity ([M/H]), and the relative abundances of α elements ([α/M])[101], carbon ([C/M]), and nitrogen ([N/M]). The micro-turbulence quoted in the DR10 results is not an independent quantity, but is instead calculated directly from the value of $\log g$. Figure 10 shows an example ASPCAP fit to an APOGEE spectrum of a typical star. ASPCAP will be fully described in an upcoming paper (A. García Pérez et al., 2014, in preparation).

Chemical composition parameters are defined as follows. The abundance of a given element X is defined relative to solar values in the standard way:

$$[X/H] = \log_{10}(n_X/n_H)_{\rm star} - \log_{10}(n_X/n_H)_\odot, \quad (1)$$

where n_X and n_H are respectively the numbers of atoms of element X and hydrogen, per unit volume, in the stellar photosphere. The parameter [M/H] is defined as an overall metallicity scaling, assuming the solar abundance pattern. The deviation of the abundance of element X from that pattern is given by

$$[X/M] = [X/H] - [M/H]. \quad (2)$$

The α elements considered in the APOGEE spectral libraries are O, Ne, Mg, Si, S, Ca, and Ti, and [α/H] is defined as an overall scaling of the abundances of those elements, where they are assumed to vary together while keeping their relative abundances fixed at solar ratios. For DR10, we allow four chemical composition parameters to vary: the overall metallicity, and the abundances of α elements, carbon, and nitrogen. Carbon, nitrogen, and oxygen contribute significantly to the opacity in APOGEE spectra of cool giants, particularly in the form of molecular lines due to OH, CO, and CN.

3.7.1. Parameter Accuracies

Mészáros et al. (2013) have compared the outputs of ASPCAP to stellar parameters in the literature for stars targeted by APOGEE in open and globular clusters spanning a wide range in metallicity. These comparisons uncovered small systematic differences between ASPCAP

---

[101] The relative α-element abundance is labeled ALPHAFE in the DR10 tables and files, but it is more accurately the ratio of the α elements to the overall metallicity, [α/M].

and literature results, which are mostly based on high-resolution optical spectroscopy. These differences are not entirely understood yet, and we hope they will be corrected in future data releases. In the meantime, calibrations have been derived to bring APOGEE and literature values into agreement. With these offsets in place, the APOGEE metallicities are accurate to within 0.1 dex for stars of S/N > 100 per half-resolution element that lie within a strict range of $T_{\rm eff}$, $\log g$, and [M/H]. Based on observed scatter in the ASPCAP calibration clusters, we estimate that the internal precision of the APOGEE measurements is 0.2 dex for $\log g$, 150 K for $T_{\rm eff}$, and 0.1 dex for $[\alpha/{\rm M}]$ (see Mészáros et al. 2013, for details).

Because most of the observed cluster stars are giants, the applied calibration offsets only apply to giants. The parameters of dwarfs are generally accurate enough to determine that they are indeed higher surface gravity stars, but otherwise their parameters are likely to be more uncertain: one reason for this is that rotation is likely to be important for a larger fraction of these stars, and the effects of rotation are not currently included in our model spectral libraries.

APOGEE mean values per cluster of $[\alpha/{\rm M}]$ are in good agreement with those in the literature. However, there are systematic correlations between $[\alpha/{\rm M}]$ and both [M/H] and $T_{\rm eff}$ for stars outside the range $-0.5 \leq [{\rm M/H}] \leq 0.1$. Moreover, important systematic effects may be present in $[\alpha/{\rm M}]$ for stars cooler than $T_{\rm eff} \sim 4200$ K. We therefore discourage use of $[\alpha/{\rm M}]$ for stars with $T_{\rm eff} < 4200$ K or with [M/H] < -0.5 or [M/H] $> +0.1$.

Figure 15 in Mészáros et al. (2013) shows the root-mean square scatter in $[\alpha/{\rm M}]$ for red giants in open and globular clusters, as a measure of the uncertainty in this parameter. However, given the trends in $[\alpha/{\rm M}]$ with other stellar parameters, care should be taken when estimating the accuracy of $[\alpha/{\rm M}]$.

Comparison with literature values for carbon and nitrogen abundances shows large scatter and significant systematic differences. In view of the relative paucity and uncertainty of literature data for these elements, more work is needed to understand these systematic and random differences before APOGEE abundances for carbon and nitrogen can be confidently adopted in science applications.

3.7.2. ASPCAP Outputs

In DR10, we provide calibrated values of effective temperature, surface gravity, overall metallicity, and $[\alpha/{\rm M}]$ for giants. In addition, we provide the raw ASPCAP results (uncalibrated, and thus, to some extent, unvalidated) for all six parameters for all stars with survey-quality data. Since commissioning data have lower resolution, different spectral libraries are needed to derive stellar parameters from them, and therefore ASPCAP results are not provided for these spectra at this time. For all stars with ASPCAP results, we also provide information about the quality of the fit (χ^2) and several bitmasks (APOGEE_ASPCAPFLAG and APOGEE_PARAMFLAG) that flag several conditions that may cause the results to be less reliable. Among these conditions are abnormally high χ^2 in the fit, best-fit parameters near the edges of the searched range, evidence in the spectrum of significant stellar rotation, and so on. Users should check the

values of these bitmasks before using the ASPCAP parameters.

Figure 11 shows the distribution of stellar properties derived by ASPCAP for stars included in DR10. The ASPCAP spectral libraries are currently only calibrated in the range $3610 < T_{\rm eff} < 5255$ K. Thus the reliable ASPCAP $T_{\rm eff}$ reported values lie only in this range, with a peak at about 4800 K. The surface gravity distribution peaks at $\log g \sim 2.5$, corresponding to red clump stars, and is strongly correlated with surface temperature. The ASPCAP models are calibrated in the range $-0.5 < \log g < 3.6$, which is reflected in the range shown. Because of the strong concentration of targeted fields to the Galactic plane (Figure 1), the metallicity distribution peaks just below solar levels, with a tail extending from [M/H] ~ -0.5 to below -2.3. The $[\alpha/{\rm M}]$ abundance distribution has both α-rich and α-poor stars, which reflects the variety of populations explored by APOGEE.

Figure 12 shows the excellent agreement of the ASPCAP $\log g$, $T_{\rm eff}$, and [M/H] values with the isochrone models of Bressan et al. (2012).

3.8. APOGEE Data Products

The APOGEE data as presented in DR10 are available as the individual 500-second spectra taken on a per-exposure basis (organized both by object and by plate+MJD+fiber), as combined co-added spectra on a per-object basis, and as continuum-normalized spectra used by the APOGEE pipeline (ASPCAP) when it computes stellar properties (Section 3.7). The individual raw exposure files, processed spectra, and combined summary files of stellar parameters are provided as FITS[102] files (Wells et al. 1981) through the DR10 Science Archive Server (SAS). The DR10 Catalog Archive Server (CAS) provides the basic stellar parameters (including the radial velocity) from the APOGEE spectra on a per-visit (SQL table apogeeVisit) and a co-added star basis (SQL table apogeeStar). The ASPCAP results are provided in the SQL table aspcapStar; the covariances between these parameters are given in a separate table, aspcapStarCovar.

To allow one to recreate the sample selection, all of the parameters used in selecting APOGEE targets are provided in DR10 in the SQL table apogeeObject.

Example queries for APOGEE data using the CAS are provided as part of the DR10 web documentation[103].

4. THE BARYON OSCILLATION SPECTROSCOPIC SURVEY (BOSS)

An overview of the BOSS survey is presented in detail in Dawson et al. (2013), and the instrument is described in Smee et al. (2013). BOSS is obtaining spectra of 1.5 million galaxies (Ahn et al. 2012), and 150,000 quasars with redshifts between 2.15 and 3.5 (Ross et al. 2012), selected from 10,000 deg^2 of SDSS imaging data. The large-scale distribution of galaxies and the structure in the quasar Lyman α forest, allow measurements of the baryon oscillation signature as a function of redshift (Anderson et al. 2012, 2013; Busca et al. 2013). In addition, about 5% of the fibers are devoted to a series of ancillary
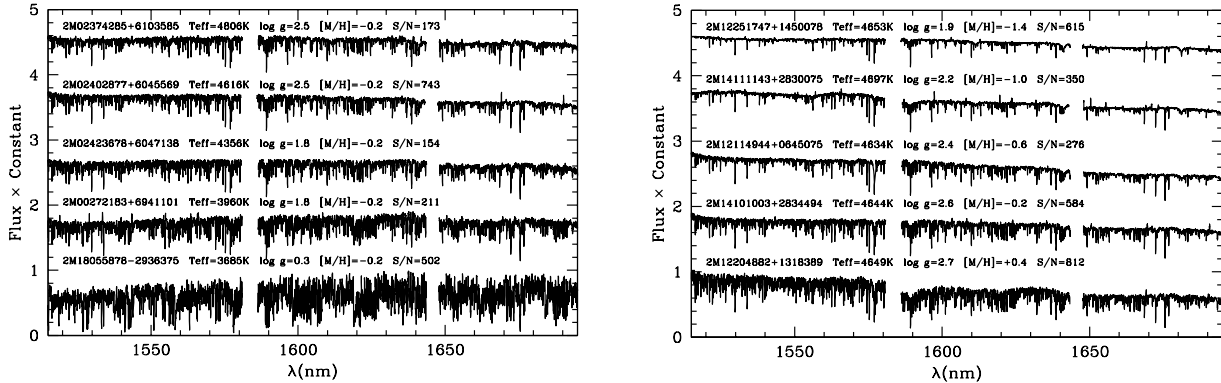
---

[102] http://fits.gsfc.nasa.gov/
[103] http://www.sdss3.org/dr10/irspec/catalogs.php#examples

Figure 9. Typical APOGEE spectra at high S/N. (left) Spectra of stars with 5000 K> T_{eff} > 3750 K at constant [M/H]= −0.2 (a characteristic [M/H] for the sample). The trend in line intensity from top to bottom is driven by decreasing T_{eff} (which is strongly correlated with $\log g$ – see Figure 11). (right) Spectra of stars with −1.4 <[M/H]< +0.4 at constant $T_{\mathrm{eff}} \sim$ 4650 K (a characteristic T_{eff} for the sample). The trend of increasing absorption lines in the spectra from top to bottom is driven by the increasing [M/H]. All of these spectra have a reported S/N of at least 200 per co-added re-sampled pixel: each of the observed absorption lines in the spectra are real features of the observed stars. The apparent emission lines are actually residuals from the incomplete subtraction of airglow lines.

Figure 10. (upper lines) An example ASPCAP fit (red) to a typical APOGEE co-added stellar spectrum (black). (lower lines) Residual of the ASPCAP model fit compared to the data (offset from zero by +0.4 units for clarity of presentation). (inset) Zoom on a region showing the high resolution of the actual data. The H-band spectrum contains a wealth of information about the elemental abundances and stellar parameters of the star. The high resolution and high S/N of APOGEE spectra allow these atmospheric properties to be measured for the entire APOGEE sample.

programs with a broad range of science goals (see the Appendix of Dawson et al. 2013).

DR9 included about 830,000 BOSS spectra over 3275 deg^2 from 1.5 years of observation; DR10 adds an additional 679,000 spectroscopic observations over 3100 deg^2 from an additional year of observation that featured unusually good weather at APO. The quality of the data is essentially unchanged from DR9. The spectra cover the wavelength range 3650–10,400Å, with a resolution of roughly $R \sim 1800$. The S/N is of course a strong function of magnitude, but at a model magnitude of $i = 19.9$, the magnitude limit of the CMASS galaxy sample (see Dawson et al. 2013; Ahn et al. 2012), the typical median S/N per pixel across the spectra is about 2. The majority of these spectra are of adequate quality for classification and measurement of a redshift; 6% of the galaxy target spectra and 12% of the quasar target spectra are flagged by the spectroscopic pipeline (Bolton et al. 2012) as having uncertain classification. These numbers are significantly higher than they were for SDSS-I/II, as the targets are quite a bit fainter, but

they remain small enough for quantitative analysis of the samples (especially with visual inspections of the quasar targets; see Pâris et al. 2012).

Figure 13 shows the sky coverage of the BOSS spectroscopic survey in more detail than in Figure 2. The tiling of the individual circular plates is visible in this completeness map of the CMASS galaxy sample. Because of the finite extent of the cladding around fibers, no two fibers can be placed closer than 62″, meaning that spectroscopy will be only about 94% complete in regions covered by only a single plate.

Figure 14 shows the distribution of DR10 BOSS spectroscopy as a function of lookback time, or equivalently redshift. The galaxy distribution peaks at a redshift of 0.5 (about 5.5 Gyr ago), with very few galaxies above redshift 0.7. By design, the majority of quasars lie between redshifts 2.15 and 3.5, as this is the range in which the Lyman α forest enters the BOSS spectral coverage.

These distributions are shown in more detail in Figure 15, which compares the redshift distributions of galaxies and quasars to those from the SDSS-I/II Legacy survey. The SDSS-I/II galaxy survey includes a magnitude-limited sample with median redshift $z \approx 0.10$ (Strauss et al. 2002) and a magnitude- and color-selected sample of luminous red galaxies extending to beyond $z = 0.4$ (Eisenstein et al. 2001). The SDSS-I/II quasar survey (Richards et al. 2002; Schneider et al. 2010) selects quasars at all redshifts and is flux-limited at magnitudes significantly brighter than BOSS; the bulk of the resulting quasar sample lies below $z = 2$. The BOSS DR10 galaxy sample is roughly the same size as the full DR7 Legacy galaxy sample (at almost five times the median redshift) and the BOSS DR10 quasar sample is significantly larger than its Legacy counterpart. DR10 includes about 60% of the full BOSS footprint, so DR12, the final SDSS-III data release, will be roughly 50% larger.

In what follows, Section 4.1 describes a new quasar target class for quasars selected using WISE data, Section 4.2 describes minor updates to the BOSS spectroscopic pipeline in DR10, and Section 4.3 discusses additions to measurements of parameters from galaxy spectra.

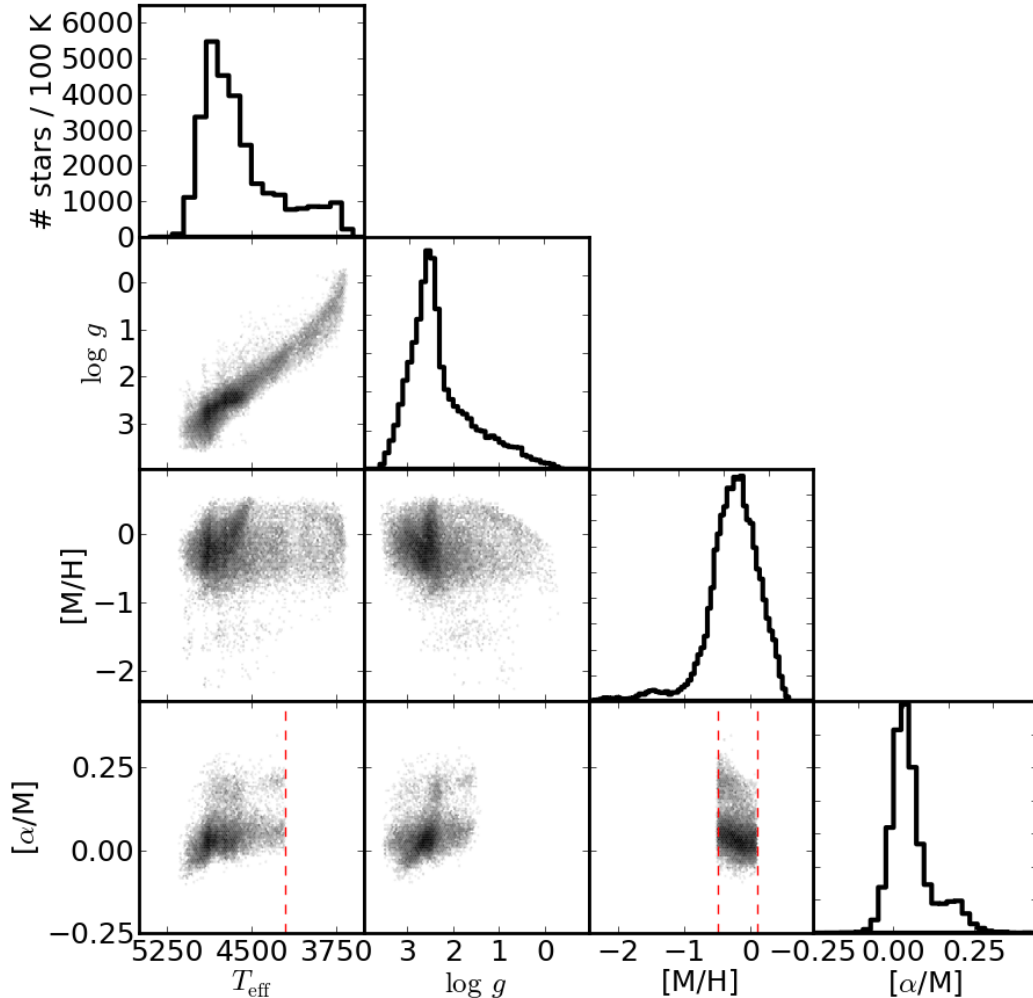### 4.1. A New Quasar Target Class in DR10

Figure 11. The one-dimensional and two-dimensional distributions of APOGEE stellar parameters — temperatures, surface gravities, metallity, and [α/M] — for all 29,438 APOGEE stars in DR10 which have reliable ASPCAP fits. The [α/M] values are only shown for the 16,066 star subset with $T_{\rm eff} > 4200$ K and $-0.5 <$[M/H]$< +0.1$, which is the range for which [α/M] values are reliable (limits are indicated by red dashed lines; see Section 3.7 for details). These distributions show what APOGEE has observed and ASPCAP has analyzed. They do not represent a fair sample of the underlying Galactic populations.

Ross et al. (2012) describe the quasar target selection used in BOSS. DR10 includes one new quasar target class, BOSS_WISE_SUPP, which uses photometry from SDSS and WISE to select $z > 2$ quasars that the standard BOSS quasar target selection may have missed, and to explore the properties of quasars selected in the infrared.

These objects were required to have detections in the 3.6 μm, 4.5 μm, and 12 μm bands, and to be point sources in SDSS imaging. They were selected with the following color cuts:

$$(u - g) > 0.4 \text{ and } (g - r) < 1.3. \qquad (3)$$

The requirement of a 12 μm detection removes essentially all stellar contamination, without any WISE color cuts.

There are 5,007 spectra from this sample in DR10, with a density of ~ 1.5/deg^2 over the $\sim 3,100$ deg^2 of new area

added by BOSS in DR10. Almost 3000 of these objects are spectroscopically confirmed to be quasars, with redshifts up to $z = 3.8$. Nine-hundred ninety-nine of these objects have $z > 2.15$.

Given the use of WISE photometry in target selection, we have imported the WISE All-Sky Release catalog (Cutri et al. 2012) into the SDSS Catalog Archive Server (CAS), and performed an astrometric cross-match with $4''$ matching radius with the SDSS catalog objects. We find no systematic shift between the WISE and SDSS astrometric systems; $4''$ extends well into the tail of the match distance distribution. The results of this matching are also available as individual files in the Science Archive Server (SAS).

4.2. *Updates to BOSS Data Processing*

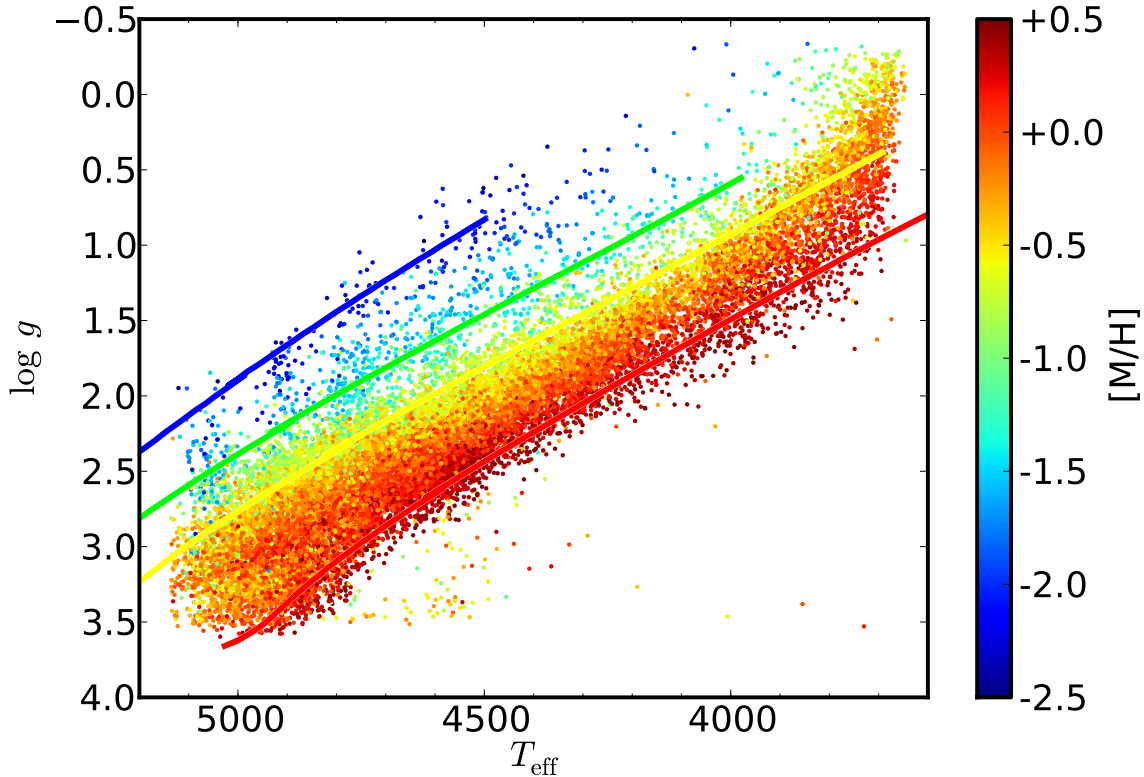We have become aware of transient hot columns on the spectrograph CCDs. Because fiber traces lie approx-

Figure 12. ASPCAP $\log g$ vs. T_{eff} with the points color-coded by [M/H]. Overplotted are isochrones for a 4 Gyr population of RGB stars with $[\alpha/\mathrm{Fe}] = 0$ from Bressan et al. (2012) on the same color-coded metallicity scale. The isochrones are for $[\mathrm{M/H}] = -1.9, -1.0, -0.58,$ and $+0.14$ from left to right.
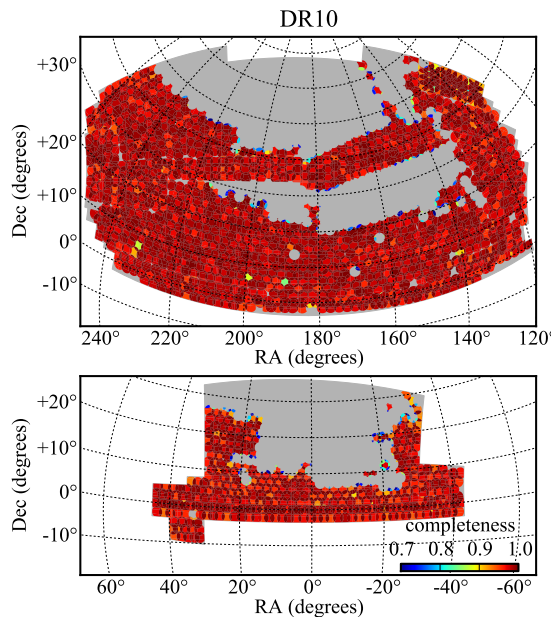

Figure 13. BOSS DR10 spectroscopic sky coverage in the Northern Galactic Cap (top) and Southern Galactic Cap (bottom). The grey region is the coverage goal for the final survey, totaling 10,000 deg^2. The color coding indicates the fraction of CMASS galaxy targets that receive a fiber; the fact that no two fibers can be placed closer than 62″ on a given plate reduces the average completeness to 94%. Note the higher completeness on the Equator in the Southern Galactic Cap (Stripe 82) where the plates are tiled with more overlapping area to recover collided galaxies.

Figure 14. The distribution of BOSS DR10 spectroscopic objects versus lookback time for the 144,968 unique stars; 859,322 unique galaxies; and 166,300 unique quasars. Lookback time is based on the observed redshift under the assumption of a ΛCDM cosmology (Komatsu et al. 2011). This figure is nearly identical to the equivalent for DR9 (Figure 3 of Ahn et al. (2012)), scaled by a factor of 1.8.

imately along columns, a bad column can adversely affect a large swath of a given spectrum. With this in mind, unusual-looking spectra associated with fibers 40, 556, and 834 and fibers immediately adjacent should be treated with suspicion; these objects are often erroneously classified as $z > 5$ quasars. We will improve the masking of these bad columns in future data releases.

We have identified 2748 objects with spectra whose astrometry is unreliable in the SDSS imaging due to tracking or focus problems of the SDSS telescope while scanning. As a consequence, the fibers may be somewhat offset from the true position of the object, often missing
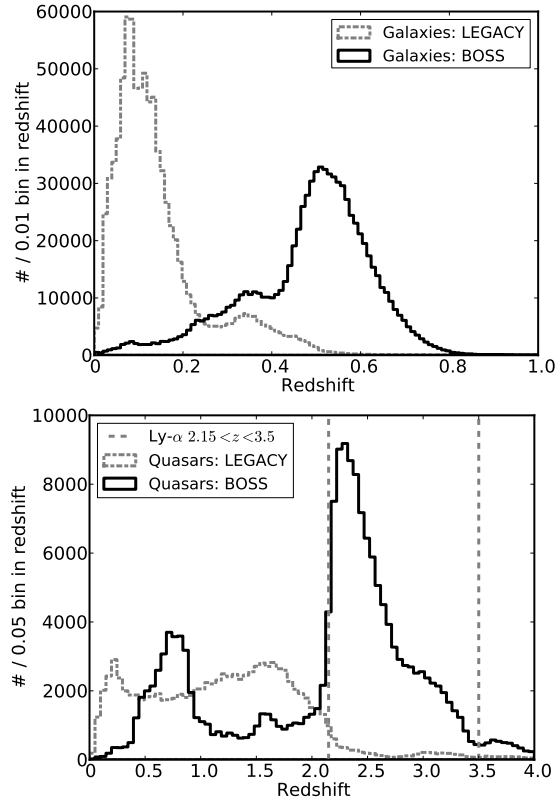
Figure 15. $N(z)$ of SDSS-III BOSS spectra in DR10 compared to that of the SDSS-I/II Legacy spectra for galaxies (top) and quasars (bottom).

it entirely (and thus having a spectrum with no signal). The redshift determination of each object is accompanied by a warning flag, ZWARNING, which indicates that the results are not reliable (Table 2 of Dawson et al. 2013). Objects with bad astrometry are assigned bit 8, BAD_TARGET in ZWARNING.

4.3. *Updates to BOSS Galaxy Stellar Population Parameters*

Estimating stellar population properties for galaxies from SDSS spectra continues to be an active field with different valid approaches. DR9 included various estimates of stellar population parameters, including:

- "Portsmouth" stellar masses derived from spectroscopic redshifts plus the SDSS imaging *ugriz* (Maraston et al. 2013);

- "Portsmouth" measurements of stellar kinematics and emission-line fluxes combined with model spectral fits to the full spectra (Thomas et al. 2013), and

- "Wisconsin" principal component analysis (PCA) of the stellar populations using fits to the wavelength range $\lambda = 3700$–5500 Å (Chen et al. 2012).

The latter two spectral fits include estimates of stellar velocity dispersions. These measurements agree with each other and the pipeline estimates of Bolton et al. (2012) within their measurement errors, but slight systematic offsets remain. For a detailed comparison we refer the reader to Thomas et al. (2013).

All stellar population calculations use the WMAP7 ΛCDM cosmology with $H_0 = 70$ km/s/Mpc, $\Omega_M = 0.274$, and $\Omega_\Lambda = 0.726$ (Komatsu et al. 2011).

In DR9, these models were calculated just for BOSS spectra; in DR10 they are extended to the $\sim 930,000$ galaxy spectra from SDSS-I/II. The Portsmouth code results in DR10 now also include the full stellar mass probability distribution function for each spectrum. The Wisconsin PCA code in DR9 used the stellar population model of Bruzual & Charlot (2003). In DR10, we have added the stellar population synthesis model of Maraston & Strömbäck (2011). In addition, the covariance matrix in the flux density in neighboring pixels due to errors in spectrophotometry has been updated by using all of the repeat galaxy observations in DR10, rather than the 5,000 randomly selected repeat galaxy observations used in DR9. This covariance is important in fitting stellar population models to the spectra.

In DR9 we also provided measurements of emission-line fluxes and equivalent widths as well as gas kinematics (Thomas et al. 2013). However, the continuum fluxes as listed in the Portsmouth DR9 catalog needed to be corrected to rest-frame by multiplication by $1 + z$. Consequently, the equivalent widths needed to be divided by the same factor $1 + z$ to be translated into the rest frame. In DR10, the continuum fluxes and equivalent widths have these correction factors applied, and are presented in the rest-frame.

In DR10, we also include results from the Granada Stellar Mass code (A. Montero-Dorta et al., 2014, in preparation) based on the publicly available "Flexible Stellar Population Synthesis" code of Conroy et al. (2009). The Granada FSPS product follows a similar spectrophotometric SED fitting approach as that of the Portsmouth galaxy product, but using different stellar population synthesis models, with varying star formation history (based on simple τ-models), metallicity and dust attenuation. The Granada FSPS galaxy product provides spectrophotometric stellar masses, ages, specific star formation rates, and other stellar population properties, along with corresponding errors, for eight different models, which are generated by applying simple, physically motivated priors to the parent grid. These eight models are based on three binary choices: (1) including or not including dust; (2) using the Kroupa (2001) vs. the Salpeter (1955) stellar initial mass function; and (3) two different configurations for the galaxy formation time: either the galaxy formed within the first 2 Gyr following the Big Bang ($z \sim 3.25$), or the galaxy formed between the time of the Big Bang and two Gyr before the observed redshift of the galaxy.

5. DATA DISTRIBUTION

All Data Release 10 data are available through data access tools linked from the DR10 web site.[104] The data are stored both as individual files in the Science Archive Server (SAS) and as a searchable database in the Catalog Archive Server (CAS). Both of these data servers have front-end web interfaces, called the "SAS Webapp"[105] and "SkyServer"[106], respectively. A number of different

[104] http://www.sdss3.org/dr10/
[105] http://data.sdss3.org/
[106] http://skyserver.sdss3.org/dr10/

interfaces are available, each designed to accomplish a specific task.

- Color images of regions of the sky in JPEG format (based on the g, r and i images; see Lupton et al. 2004) can be viewed in a web browser with the SkyServer Navigate tool. These are presented at higher resolution, and with greater fidelity, than in previous releases. With DR10 we also include JPEG images of the 2MASS data to complement the APOGEE spectra.

- FITS images can be searched for, viewed, and downloaded through the SAS Webapp.

- Complete catalog information (astrometry, photometry, etc.) of any imaging object can be viewed through the SkyServer Explore tool.

- Individual spectra, both optical and infrared, can be searched for, viewed, and downloaded through the SAS Webapp.

- Catalog search tools are available through the Sky-Server interface to the CAS, each of which returns catalog data for objects that match supplied criteria. For more advanced queries, a powerful and flexible catalog search website called "CasJobs" allows users to create their own personalized data sets and then to modify or graph their data.

Links to all of these methods are provided at http://www.sdss3.org/dr10/data_access/.

The DR10 web site also features data access tutorials, a glossary of SDSS terms, and detailed documentation about algorithms used to process the imaging and spectroscopic data and select spectroscopic targets.

Imaging and spectroscopic data from all prior data releases are also available through DR10 data access tools, with the sole caveat that the 303 imaging runs covering the equatorial stripe in the Fall sky ("Stripe 82") are only fully provided in DR7[107] – only the good quality images are included from Stripe 82 in DR8 and subsequent releases.

6. FUTURE

The SDSS-III project will present two more public data releases: DR11 and DR12, both to be released in December 2014. DR11 will include data taken through the summer of 2013. DR12 will be the final SDSS-III data release and will include the final data through Summer 2014 from all observations with APOGEE, BOSS, MAR-VELS, and SEGUE-2.

In 2014 July, operation of the 2.5-m Sloan Foundation Telescope will be taken over by the next generation of SDSS, currently known as SDSS-IV, which plans to operate for six years. SDSS-IV consists of three surveys mapping the Milky Way Galaxy, the nearby galaxy population, and the distant universe. APOGEE-2 will continue the current APOGEE program of targeting Milky Way stars to study Galactic archaeology and stellar astrophysics. It will include a southern component, observing from the 2.5-m du Pont Telescope at Las Campanas Observatory, Chile, allowing a full-sky view of the structure of the Milky Way. Mapping Nearby Galaxies at APO (MaNGA) will use the BOSS spectrograph in a new mode, bundling fibers into integral field units to observe 10,000 nearby galaxies with spatially resolved spectroscopy. MaNGA has already observed a small number of targets using BOSS time to test its planned hardware configuration. Finally, the Extended Baryon Oscillation Spectroscopic Survey (eBOSS) will create the largest volume three-dimensional map of the universe to date, to measure baryon acoustic oscillations and constrain cosmological parameters in the critical and largely unexplored redshift range $0.6 < z < 2.1$. eBOSS will also obtain spectra of X-ray sources detected by the eROSITA satellite (Predehl et al. 2010), as well as of variable stars and quasars to understand their physical nature. The SDSS-IV collaboration will continue the production and distribution of cutting-edge and diverse data sets through the end of the decade.

REFERENCES

Abazajian, K., et al. 2004, AJ, 128, 502
Abazajian, K., et al. 2005, AJ, 129, 1755
Abazajian, K., et al. 2003, AJ, 126, 2081
Abazajian, K. N., et al. 2009, ApJS, 182, 543
Adelman-McCarthy, J. K., et al. 2008, ApJS, 175, 297
Adelman-McCarthy, J. K., et al. 2007, ApJS, 172, 634
Adelman-McCarthy, J. K., et al. 2006, ApJS, 162, 38

[107] http://skyserver.sdss.org/dr7

18

Ahn, C. P., et al. 2012, ApJS, 203, 21
Aihara, H., et al. 2011, ApJS, 193, 29
Anderson, L., et al. 2013, ArXiv e-prints, 1303.4666
Anderson, L., et al. 2012, MNRAS, 427, 3435
Annis, J., et al. 2011, ArXiv e-prints, 1111.6619
Benjamin, R. A., et al. 2003, PASP, 115, 953
Bolton, A. S., et al. 2012, AJ, 144, 144
Borucki, W. J., et al. 2010, Science, 327, 977
Bovy, J., et al. 2012, ApJ, 759, 131
Bressan, A., et al. 2012, MNRAS, 427, 127
Bruzual, G., & Charlot, S. 2003, MNRAS, 344, 1000
Busca, N. G., et al. 2013, A&A, 552, A96
Canterna, R. 1976, AJ, 81, 228
Chaplin, W. J., & Miglio, A. 2013, ARA&A, 51, 353
Chen, Y.-M., et al. 2012, MNRAS, 421, 314
Churchwell, E., et al. 2009, PASP, 121, 213
Clark, J. P. A., & McClure, R. D. 1979, PASP, 91, 507
Conroy, C., Gunn, J. E., & White, M. 2009, ApJ, 699, 486
Cutri, R. M., et al. 2012, Explanatory Supplement to the WISE
  All-Sky Data Release Products, Tech. rep.
Dawson, K. S., et al. 2013, AJ, 145, 10
Eisenstein, D. J., et al. 2001, AJ, 122, 2267
Eisenstein, D. J., et al. 2011, AJ, 142, 72
Frieman, J. A., et al. 2008, AJ, 135, 338
Fukugita, M., et al. 1996, AJ, 111, 1748
García Pérez, A. E., et al. 2013, ApJ, 767, L9
Garnett, J. D., et al. 2004, in Society of Photo-Optical
  Instrumentation Engineers (SPIE) Conference Series, Vol. 5499,
  Society of Photo-Optical Instrumentation Engineers (SPIE)
  Conference Series, ed. J. D. Garnett & J. W. Beletic, 35–46
Gilliland, R. L., et al. 2010, PASP, 122, 131
Gunn, J. E., et al. 1998, AJ, 116, 3040
Gunn, J. E., et al. 2006, AJ, 131, 2332
Hekker, S., et al. 2011, A&A, 530, A100
Indebetouw, R., et al. 2005, ApJ, 619, 931
Ivezić, Ž., et al. 2004, Astronomische Nachrichten, 325, 583
Komatsu, E., et al. 2011, ApJS, 192, 18
Kroupa, P. 2001, MNRAS, 322, 231
Lintott, C., et al. 2011, MNRAS, 410, 166
Lintott, C. J., et al. 2008, MNRAS, 389, 1179
Lupton, R., et al. 2004, PASP, 116, 133

Lupton, R., et al. 2001, in Astronomical Society of the Pacific
  Conference Series, Vol. 238, Astronomical Data Analysis
  Software and Systems X, ed. F. R. Harnden, Jr., F. A. Primini,
  & H. E. Payne, 269
Majewski, S. R., Ostheimer, J. C., Kunkel, W. E., & Patterson,
  R. J. 2000, AJ, 120, 2550
Majewski, S. R., Zasowski, G., & Nidever, D. L. 2011, ApJ, 739,
  25
Maraston, C., et al. 2013, MNRAS
Maraston, C., & Strömbäck, G. 2011, MNRAS, 418, 2785
Mészáros, S., et al. 2012, AJ, 144, 120
Mészáros, S., et al. 2013, AJ, 146, 133
Nidever, D. L., et al. 2012, ApJ, 755, L25
Padmanabhan, N., et al. 2008, ApJ, 674, 1217
Pâris, I., et al. 2012, A&A, 548, A66
Pâris, I., et al. 2013, A&A *in press*, ArXiv e-prints, 1311.4870
Pier, J. R., et al. 2003, AJ, 125, 1559
Predehl, P., et al. 2010, in Society of Photo-Optical
  Instrumentation Engineers (SPIE) Conference Series, Vol. 7732,
  Society of Photo-Optical Instrumentation Engineers (SPIE)
  Conference Series
Richards, G. T., et al. 2002, AJ, 123, 2945
Rieke, G. H. 2007, ARA&A, 45, 77
Ross, N. P., et al. 2012, ApJS, 199, 3
Salpeter, E. E. 1955, ApJ, 121, 161
Schneider, D. P., et al. 2010, AJ, 139, 2360
Skrutskie, M. F., et al. 2006, AJ, 131, 1163
Smee, S. A., et al. 2013, AJ, 146, 32
Stoughton, C., et al. 2002, AJ, 123, 485
Strauss, M. A., et al. 2002, AJ, 124, 1810
Thomas, D., et al. 2013, MNRAS, 431, 1383
Tucker, D. L., et al. 2006, Astronomische Nachrichten, 327, 821
Wells, D. C., Greisen, E. W., & Harten, R. H. 1981, A&AS, 44,
  363
Willett, K. W., et al. 2013, MNRAS, 435, 2835
Wright, E. L., et al. 2010, AJ, 140, 1868
Yanny, B., et al. 2009, AJ, 137, 4377
York, D. G., et al. 2000, AJ, 120, 1579
Zasowski, G., et al. 2013, AJ, 146, 81